Direction Finding Arrays in Acoustic and Electromagnetic Domains

Submitted by
Huang Yongchang

Department of Electrical & Computer Engineering

In partial fulfillment of the
requirements for the Degree of
Bachelor of Engineering
National University of Singapore

ABSTRACT

In this thesis, we consider the problem of direction finding in the acoustic and electromagnetic domain. In the electromagnetic domain, Maximum Ratio Combining (MRC) and Median Filtering have been proposed as the appropriate wideband DOA techniques that can be used in a frequency selective channel and in the presence of narrowband interferences. Simulation results have shown that these proposed techniques yield a more accurate Direction of Arrival (DOA) estimation in comparison to Equal Gain Combining (EGC). The narrowband MUSIC algorithm has also been tested in the antenna test chamber at Temasek Laboratories. Implementation issues involving the calibration of multiple software-defined radios have been resolved using a calibration signal for phase estimation and phase compensation. In the acoustic domain, sophisticated direction finding algorithms have been developed on an Autonomous Underwater Vehicle (AUV) to complete the acoustic localization task in the Singapore AUV Challenge (SAUVC). Results collected from extensive pool tests indicate that the high-resolution MUSIC algorithm presents a more robust solution compared to the Time Difference of Arrival (TDOA) algorithm.

ACKNOWLEDGEMENTS

I wish to thank my dedicated supervisors Professor Lim Teng Joon and Dr Ong Lay Teen for their support throughout the course of this project. Their expertise in the field of signal processing and electromagnetics has accelerated my learning, giving me time to deliver innovative solutions to practical problems in direction finding. I would also like to thank Assistant Professor Mandar Chitre, Head of the Acoustic Research Laboratory, for his guidance in the field of acoustic signal processing.

I would like to acknowledge the technical support given by Mr Tan Pheng Khiang and Mr Dylan Ang Chin Keong, Lab Technologists of the Antenna Group of Electromagnetic Division at Temasek Laboratories.

Special thanks should be given to Thomas Ng, the captain of Team Bumblebee, for giving me the opportunity to extend my work to the acoustic domain. I am particularly grateful to all the members from team for their help and support over the past few months.

I would also like to thank the equipment sponsors National Instruments and Teledyne Reson for providing the necessary hardware to design the acoustic sub-system.

CONTENTS

LIST OF FIGURES

LIST OF TABLES

LIST OF SYMBOLS AND ABBREVIATIONS

M	Number of Elements in an Array
$\widehat{D}$	Number of Point Sources
a	Baseband Phase Shift
$r(t)$	Received Signal
$S(t)$	Transmitted Signal
$n(t)$	Additive White Gaussian Noise
$\boldsymbol{r}$	Received Signal Vector
$\boldsymbol{A}$	Array Steering Vector or Array Manifold
$\boldsymbol{s}$	Transmitted Signal Vector
$\boldsymbol{n}$	Noise Vector
λ	Wavelength of Source
l	Path Difference
τ_m	Time Delay between $r_m(t)$ and $r_1(t)$
f	Frequency of Source
d	Inter-element Spacing
c	Speed of Light
θ	Direction of Arrival (Azimuth)
ϕ	Direction of Arrival (Elevation)
ω	Angular Frequency of Source
$\mathbf{R}$	Spatial Covariance Matrix
$\mathbf{I}$	Identity Matrix
σ^2	Variance of Noise
$\boldsymbol{T}$	Number of Samples

$\boldsymbol{v_i}$	Eigenvectors
$\boldsymbol{\lambda_x}$	Eigenvalues
$\boldsymbol{K}$	Multiplicity of K
$\boldsymbol{V_n}$	Eigenvectors from the Noise Subspace
$\boldsymbol{\lambda_n}$	Eigenvalues from the Noise Subspace
$\boldsymbol{V_s}$	Eigenvectors from the Signal Subspace
$\boldsymbol{\lambda_s}$	Eigenvalues from the Signal Subspace
$\boldsymbol{\alpha}(\phi)$	Array Steering Vector at an angle ϕ
$\boldsymbol{\widehat{P}_{music}}$	Array of values computed from the MUSIC algorithm
$\boldsymbol{P_{cbf}}$	Array of values computed from the Fourier Method
$\boldsymbol{\Phi}$	Diagonal matrix with entries $e^{-j\frac{2\pi d sin\theta}{\lambda}}$
J_k	Selection Matrix
$\boldsymbol{T}$	Transformation Matrix
$\boldsymbol{\Psi}$	A new matrix defined as $\boldsymbol{T\Phi T^{-1}}$
$\theta(f)$	Vector of DOA from the wideband problem
$S(f)$	Power Spectral Density
$N(f)$	Noise Spectral Density
$I(f)$	Spectrum of Narrowband Interference
θ_{offset}	Phase offset between multiple USRP
Θ_{mn}	Phase difference between hydrophone m and n
$E(.)$	Expected Value
MSE	Mean Square Error
RMSE	Root Mean Square Error

CHAPTER ONE

Introduction

It is of interest to augment current research in the area of direction finding because of the numerous applications it has to offer. Three important applications are Personal Communications, Radar and Sonar, as well as Industrial Applications [1]. In the field of passive Sonar, direction finding of an acoustic pinger has been used for the search of the flight data recorder after the crash of Air France Flight 447 [2]. This research project comprises of two distinctive components: the electromagnetic and acoustic domain.

In the electromagnetic domain, the research is done in collaboration with Temasek Laboratories because location is an important parameter to the defence community. It entails developing Direction Finding techniques with direct application to wideband Radar systems.

In the acoustic domain, the direction finding algorithm is developed with Team Bumblebee. Team Bumblebee is an undergraduate AUV team founded to compete in student AUV competitions. The developed algorithm has been used to complete the acoustic localization task at SAUVC [3], organized by IEEE Oceanic Engineering Society (OES) Singapore Chapter. This algorithm will also be used in 17th Associate for Unmanned Vehicle System International (AUVSI) Robosub Competition held at San Diego, California [4].

1.1 Motivation

In electromagnetics, a wideband signal offers several advantages over narrowband signals, such as higher data rates and frequency diversity [5]. A wideband signal can be decomposed into many narrowband signals via discrete Fourier transform [6]. DOA estimates can be obtained at each frequency bin within the signal bandwidth. Consequently, these estimates could be combined using a variety of existing techniques such as the Incoherent Subspace Method (ISSM). It is believed that this would increase the accuracy of the final DOA estimate compared to the narrowband case.

Recognizing that beamforming algorithms offer an accurate DOA estimate in the electromagnetic domain, this research extends the theories to the development of an acoustic sub-system of an AUV. In the 2013 design, Team Bumblebee used the TDOA algorithm to complete the acoustic localization task [7]. The TDOA is computed from time of arrival estimates obtained from filtering and dynamic thresholding. It is observed that dynamic thresholding does not guarantee an accurate time of arrival estimate, and this has severe implications on the accuracy of the TDOA algorithm. This motivates the development of more sophisticated array signal processing techniques using the high-resolution beamforming methods.

1.2 Problem Description in the Electromagnetic Domain

Existing wideband direction finding techniques are not designed to work well when various forms of channel impairments are present. This research proposes new wideband direction finding methods in two practical scenarios.

(a) Frequency Selective Fading

A wideband signal is likely to experience frequency selective fading because the coherence bandwidth is much smaller than the signal bandwidth. Fading will cause certain frequency components to have a lower power, hence resulting in poorer DOA estimations. In combining these DOAs, it would be reasonable to allocate lower DOA weightings to frequency bins of a lower power.

(b) Narrowband Interferences

Frequency diversity is inherent in a wideband signal because it offers immunity against fading as well as narrowband interferences. When the signal of interest is narrowband, any form of interference or jamming can result in an inaccurate DOA estimation. However if the desired signal is wideband, a multi-tone jammer can only distort DOA estimates at certain frequencies.

1.3 Problem Description in the Acoustic Domain

The AUV must localize the direction of two acoustic pingers that emit one ping every second. The pingers' frequencies are set at 37.5 and 45 kHz. The acoustic signal will experience multiple reverberations from the surface, floor and tiled walls. This results in multipath interference whereby the line of sight signal is distorted by the reflected pings. An appropriate algorithm must be designed such that the AUV can resurface inside an end zone. The end zone is a 150cm by 150cm square marked on the surface, with acoustic pingers on its diagonally opposite vertices.

1.4 Background

Direction finding algorithms can be classified into three main categories: the Fourier Method and Capon's Minimum Variance, Subspace-methods and Maximum Likelihood Techniques.

(a) Fourier Method and Capon's Minimum Variance

The Fourier method [8] is a classical DOA algorithm with many disadvantages. It yields a poor resolution and requires a large array size to achieve a good performance. Capon's Minimum Variance technique [9] improved the resolution at the expense of computational cost and complexity.

(b) Subspace-methods

Subspace based methods involve the use of Eigen-decomposition and spatial covariance matrix for DOA estimation. A popular subspace based method is the MUSIC (Multiple Signal Classification) algorithm [10]. It presents a high-resolution DOA estimate. It is not computationally intensive, and only involves a 1-D search in the steering vector [1]. However, the use of MUSIC should be limited to incoherent cases, and the number of sources has to be smaller than the number of array elements. Two signals are coherent if one is a scaled and delayed version of the other. [1]

(c) Maximum Likelihood Techniques

Although subspace methods are computationally attractive, they do not yield accurate results in the presence of coherent signals [1]. Hence, maximum likelihood techniques were developed. These techniques include Deterministic Maximum Likelihood (DML) and Stochastic Maximum Likelihood (SML) [11]. However, it is complex to implement these algorithms because multi-dimensional search is often required.

In this thesis, subspace methods will be developed as they offer accurate DOA estimates, and are computationally less intensive compared to maximum likelihood techniques. Specifically, MUSIC and ESPRIT (Estimation of Signal Parameters by Rotational Invariance Techniques) [12] will be explored.

CHAPTER TWO

Literature Review

Subspace-based methods require a good understanding of fundamental concepts such as array manifold, spatial covariance matrix and Eigen-decomposition using a narrowband signal model. These concepts are applied to the proposed direction finding algorithms used in the electromagnetic and acoustic domain. The following derivation is adapted from two sources [13] [14].

2.1 Narrowband Signal Model

A classical direction finding problem is formulated based on the narrowband signal model. In array signal processing, a narrowband signal is assumed to have a fractional bandwidth of less than 1%.

(a) One Point Source, Three Antennas

Consider a case whereby there is a Uniform Linear Array (ULA) with three antennas ($M = 3$) and one point source ($\widehat{D} = 1$). The received signal vector is formulated in the following equation. The baseband phase shift of source signal $S_1(t)$ at antennas 1, 2 and 3 are represented by a_{11}, a_{12} and a_{13} respectively. The Additive White Gaussian Noise (AWGN) at receiver i is $n_i(t)$.

$$\begin{pmatrix} r_1(t) \\ r_2(t) \\ r_3(t) \end{pmatrix} = \begin{pmatrix} a_{11} \\ a_{12} \\ a_{13} \end{pmatrix} S_1(t) + \begin{pmatrix} n_1(t) \\ n_2(t) \\ n_3(t) \end{pmatrix} \dots \ (1)$$

(b) Two Point Sources, Three Antennas

Extending this to a case of M = 3 and $\widehat{D} = 2$ (Figure 1), the received signal vector is a superposition of $S_1(t)$ and $S_2(t)$ multiplied by their appropriate phase weights.

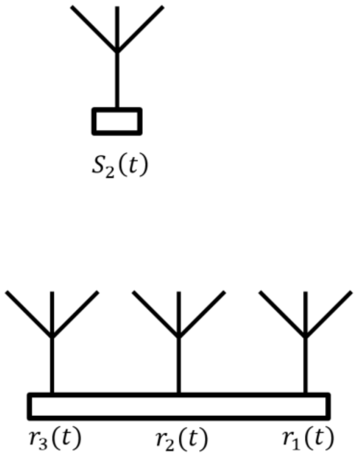

Figure 1: Uniform Linear Array (ULA) with 3 Antennas and 2 Point Sources

$$\begin{pmatrix} r_1(t) \\ r_2(t) \\ r_3(t) \end{pmatrix} = \begin{pmatrix} a_{11} \\ a_{12} \\ a_{13} \end{pmatrix} S_1(t) + \begin{pmatrix} a_{21} \\ a_{22} \\ a_{23} \end{pmatrix} S_2(t) + \begin{pmatrix} n_1(t) \\ n_2(t) \\ n_3(t) \end{pmatrix} \ldots (2)$$

$$\begin{pmatrix} r_1(t) \\ r_2(t) \\ r_3(t) \end{pmatrix} = \begin{pmatrix} a_{11} & a_{21} \\ a_{12} & a_{22} \\ a_{13} & a_{23} \end{pmatrix} \begin{pmatrix} S_1(t) \\ S_2(t) \end{pmatrix} + \begin{pmatrix} n_1(t) \\ n_2(t) \\ n_3(t) \end{pmatrix} \ldots (3)$$

(c) D Point Sources, M Antennas

For M antennas and D point sources, the received signal vector, $\boldsymbol{r}$, can be equated to the product of array steering matrix $\boldsymbol{A}$ and the transmitted signal vector $\boldsymbol{s}$, with the noise vector is added to this product.

$$\begin{pmatrix} r_1(t) \\ r_2(t) \\ * \\ * \\ r_M(t) \end{pmatrix} = \begin{pmatrix} a_{11} & a_{21} & * & a_{D1} \\ a_{12} & a_{22} & * & a_{D2} \\ * & * & * & * \\ * & * & * & * \\ a_{1M} & a_{2M} & * & a_{DM} \end{pmatrix} \begin{pmatrix} S_1(t) \\ S_2(t) \\ * \\ S_D(t) \end{pmatrix} + \begin{pmatrix} n_1(t) \\ n_2(t) \\ * \\ n_D(t) \end{pmatrix} \ldots (4)$$

$$\boldsymbol{r} = \boldsymbol{As} + \boldsymbol{n} \ldots (5)$$

2.2 Array Manifold of a Uniform Linear Array (ULA)

It is essential to derive the key parameters associated with the array manifold as required for correct modelling of the narrowband problem. Apart from the direction of arrival and inter-element spacing d, the array manifold is also dependent on the configuration of the antenna array. A ULA will be adopted in the following discussion. In order to avoid spatial aliasing, the inter-element spacing *d* must not exceed half of the carrier wavelength. i.e. $d \leq \lambda/2$

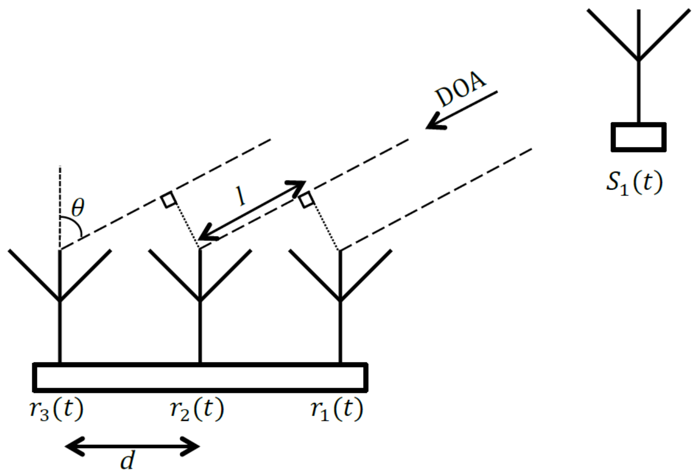

Figure 2: Parameters of Array Manifold

Assume that the signal $S_1(t)$ is a far-field point source. The path difference l between two consecutive antenna elements is:

$$l = d sin\theta \ldots (6)$$

Define a new variable τ_m to represent the time delay between the received signals $r_m(t)$ and $r_1(t)$; the value τ_m is obtained from:

$$\tau_m = \frac{(m-1)d sin\theta}{c} = \frac{(m-1)d sin\theta}{f\lambda} \ldots (7)$$

Consequently, the array manifold can be formulated. This is a complex baseband representation of a time-shifted sinusoid.

$$A = \begin{pmatrix} e^{-j\omega\tau_1} \\ e^{-j\omega\tau_2} \\ e^{-j\omega\tau_3} \end{pmatrix} \ldots (8)$$

In this array manifold, the path difference is assumed to have negligible impact on the amplitude of the received signals. However, the DOA information is carried entirely in the phase differences between antenna elements and therefore accurate phase measurements are critical in a DOA estimation application using antenna arrays. For D Signals and M Antennas, the array manifold can be represented as:

$$A = \begin{pmatrix} a_{11} & a_{21} & * & a_{D1} \\ a_{12} & a_{22} & * & a_{D2} \\ * & * & * & * \\ * & * & * & * \\ a_{1M} & a_{2M} & * & a_{DM} \end{pmatrix} = \begin{pmatrix} e^{-j\omega\tau_{11}} & e^{-j\omega\tau_{21}} & * & e^{-j\omega\tau_{D1}} \\ e^{-j\omega\tau_{12}} & e^{-j\omega\tau_{22}} & * & e^{-j\omega\tau_{D2}} \\ * & * & * & * \\ * & * & * & * \\ e^{-j\omega\tau_{1M}} & e^{-j\omega\tau_{2M}} & * & e^{-j\omega\tau_{DM}} \end{pmatrix} \ldots (9)$$

$\omega\tau_{im} = \frac{2\pi(m-1)dsin\theta_i}{\lambda}$ where θ_i is DOA of i^{th} signal

2.3 Spatial Covariance Matrix

The subspace-based methods require the computation of the Spatial Covariance Matrix, and the following section is devoted to understanding its key relationships.

Defining the covariance matrix of the received signal to be $\mathbf{R_x}$ and the covariance matrix of the array steering vector to be $\mathbf{R_A}$; then $\mathbf{R_x}$ can be expressed as a linear combination of $\mathbf{R_A}$ and the variance of the noise σ^2. The detailed derivation is available in Appendix A.

$$\mathbf{R_x} = \mathbf{R_A} + \sigma^2\mathbf{I} \ldots (10)$$

In practice, an estimated covariance matrix $\widehat{\mathbf{R_x}}$ is computed using time average of the received signal vector $\boldsymbol{r}(t)$ multiplied by its Hermitian conjugate. In order to achieve a good estimate, the value of T (i.e. number of samples) should be large.

$$\widehat{\mathbf{R_x}} = \frac{1}{T}\sum_{\boldsymbol{t}=1}^{T} \boldsymbol{r}(t)\, \boldsymbol{r}(t)^{\boldsymbol{H}} \ldots (11)$$

2.4 Eigen Decomposition

Eigen decomposition is applied on the spatial covariance matrix to obtain vectors corresponding to the signal and noise subspaces. The spatial covariance matrix can be expressed as a product of its eigenvalues and eigenvectors:

$$\boldsymbol{R_x v_i} = \boldsymbol{\lambda_x v_i} \ldots (12)$$

$\boldsymbol{R_x v_i}$ can also be expressed as $\boldsymbol{\lambda_A}\ \boldsymbol{v_i} + \sigma^2 \boldsymbol{v_i}$ (where $\boldsymbol{\lambda_A}$ is the eigenvalues of the matrix $\boldsymbol{R_A}$).

$$\boldsymbol{R_x v_i} = (\boldsymbol{R_A} + \sigma^2 \boldsymbol{I})\boldsymbol{v_i} = \boldsymbol{R_A v_i} + \sigma^2 \boldsymbol{v_i} = \boldsymbol{\lambda_A}\ \boldsymbol{v_i} + \sigma^2 \boldsymbol{v_i} \ldots (13)$$

The covariance matrix $\boldsymbol{R_A}$ has a rank of $\widehat{D}$, corresponding to the number of point sources around M antennas. This means that $\boldsymbol{\lambda_A}$, the eigenvalues of $\boldsymbol{R_A}$, consist of $\widehat{D}$ non-zero eigenvalues and $(M - \widehat{D})$ zero eigenvalues. Here, the multiplicity of *K* is defined as:

$$K = M - \widehat{D} \ldots (14)$$

From Equations (12) and (13), the eigenvalues of $\boldsymbol{R_x}$ and $\boldsymbol{R_A}$ can be expressed as:

$$\lambda_x = \lambda_A + \sigma^2 \ldots (15)$$

Since $\boldsymbol{\lambda_A}$ has *K* zero eigenvalues , $\boldsymbol{\lambda_x}$ must contain *K* minimum eigenvalues which is equivalent to the noise variance σ^2. Without loss of generality, we assume that the eigenvectors $[\boldsymbol{v_1} \quad \boldsymbol{v_2} \quad \ldots\ \boldsymbol{v_\mathrm{M}}]$ corresponds to the eigenvalues of $\lambda_1,\ \lambda_2, \ldots\ \lambda_\mathrm{M}$, such that $\lambda_1 \leq \lambda_2 \ldots \leq \lambda_\mathrm{M}$:

The eigenvectors and eigenvalues in the **noise subspace** are

$$\boldsymbol{V_n} = [\boldsymbol{V_1} \quad \boldsymbol{V_2} \ldots \boldsymbol{V_K}] \ldots (16)$$

$$\boldsymbol{\lambda_n} = [\lambda_1 \quad \lambda_2 \ldots \lambda_K] \ \ldots (17)$$

The eigenvectors and eigenvalues in the **signal subspace** are

$$\boldsymbol{V_s} = [\boldsymbol{V_{K+1}} \quad \boldsymbol{V_{K+2}} \ldots \boldsymbol{V_M}] \ldots (18)$$

$$\boldsymbol{\lambda_s} = [\lambda_{K+1} \quad \lambda_{K+2} \ldots \lambda_M] \ldots (19)$$

2.5 MUSIC Algorithm

The MUSIC algorithm [15] searches for an angle ϕ such that steering vector $\boldsymbol{\alpha}(\phi)$ is the most orthogonal to the noise eigenvectors $\boldsymbol{V_n}$. When ϕ is the DOA, the array steering vector $\boldsymbol{\alpha}(\phi)$ lies in the signal subspace. This is because any signals on the signal subspace can be expressed as a linear combination of the steering vector if and only if ϕ is the DOA of the signal.

$$\boldsymbol{\alpha}(\phi) = \begin{pmatrix} e^{-j\omega\tau_1} \\ e^{-j\omega\tau_2} \\ * \\ e^{-j\omega\tau_M} \end{pmatrix} \ldots (20)$$

$$\omega\tau_m = \frac{2\pi(m-1)dsin\phi}{\lambda} \ldots (21)$$

The MUSIC algorithm measures the orthogonality between $\boldsymbol{\alpha}(\phi)$ and $\boldsymbol{V_n}$ through the projection of the steering vector $\boldsymbol{\alpha}(\phi)$ on the noise subspace i.e. $\boldsymbol{\alpha}^H(\phi)\boldsymbol{V_n}\boldsymbol{V_n^H}\boldsymbol{\alpha}(\phi)$. If $\boldsymbol{\alpha}(\phi)$ and $\boldsymbol{V_n}$ are orthogonal, the projection of $\boldsymbol{\alpha}(\phi)$ on $\boldsymbol{V_n}$ is zero. The DOAs of the incoming signals are indicated by the peaks of $\hat{P}_{music}(\phi)$ derived from a 1-D search with angles between 0 and 180 degrees.

$$\widehat{\boldsymbol{P}}_{\boldsymbol{music}}(\phi) = \frac{\boldsymbol{\alpha^H}(\phi)\boldsymbol{\alpha}(\phi)}{\boldsymbol{\alpha^H}(\phi)\boldsymbol{V_n}\boldsymbol{V_n^H}\boldsymbol{\alpha}(\phi)} \ldots (22)$$

2.6 ESPRIT Algorithm

The ESPRIT algorithm [16] is another popular subspace based method. It is more computationally efficient compared to MUSIC because it does not require a 1-D angular search. However, it requires more antenna elements for DOA estimation. If there are D point sources, there must be at least D+2 elements. This algorithm can only be applied when the inter-element spacing is identical. Hence, its usefulness is limited to ULA.

The ULA is divided into two sub-arrays 1 and 2.

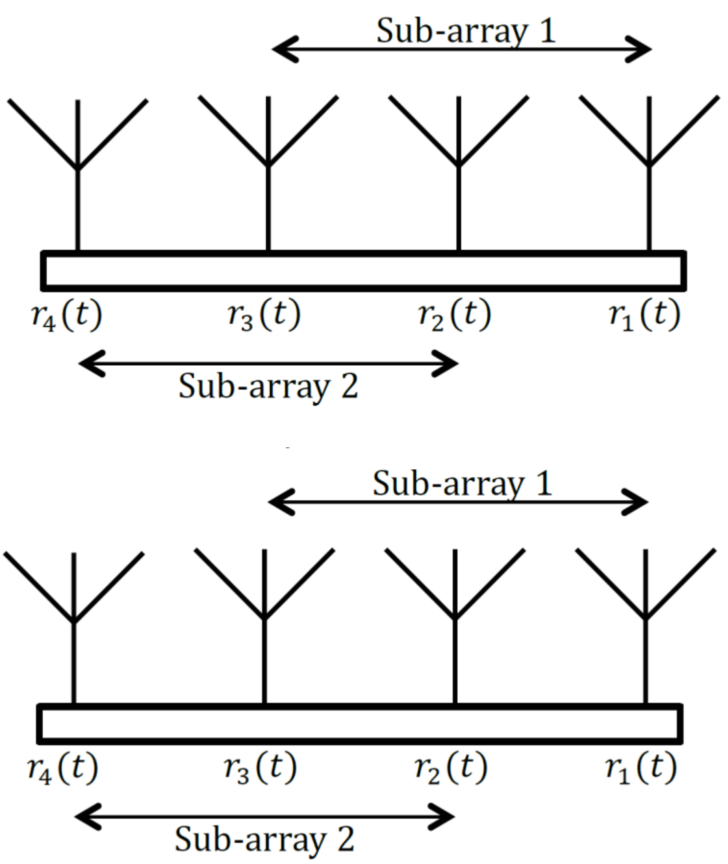

Figure 3: Sub-arrays of ESPRIT Algorithm

Entire Array: Array Manifold of $\boldsymbol{A}$

Sub-array 1: Array Manifold of $\boldsymbol{A}_1$

Sub-array 2: Array Manifold of $\boldsymbol{A}_2$

The array manifolds $\boldsymbol{A}_1$ and $\boldsymbol{A}_2$ are related by:

$$\boldsymbol{A}_2 = \boldsymbol{A}_1\boldsymbol{\Phi} \dots (23)$$

$\boldsymbol{\Phi}$ is a diagonal matrix whose main-diagonal entries are $e^{-j\frac{2\pi d sin\theta}{\lambda}}$.

Define a selection matrix J_k such that $\boldsymbol{A}_k = \boldsymbol{J}_k\boldsymbol{A}$:

$$\boldsymbol{A}_1 = \boldsymbol{J}_1\boldsymbol{A} \dots (24)$$

$$\boldsymbol{J}_1 = \begin{pmatrix} 1 & 0 & 0 & 0 \\ 0 & 1 & 0 & 0 \\ 0 & 0 & 1 & 0 \end{pmatrix} \dots (25)$$

$$\boldsymbol{A}_2 = \boldsymbol{J}_2\boldsymbol{A} \dots (26)$$

$$\boldsymbol{J}_2 = \begin{pmatrix} 0 & 1 & 0 & 0 \\ 0 & 0 & 1 & 0 \\ 0 & 0 & 0 & 1 \end{pmatrix} \dots (27)$$

Substituting Equation (24) and (26) into (23), $\boldsymbol{\Phi}$ can be expressed using the selection matrix $\boldsymbol{J}$ and array manifold $\boldsymbol{A}$:

$$\boldsymbol{J}_2\boldsymbol{A} = \boldsymbol{J}_1\boldsymbol{A}\boldsymbol{\Phi} \dots (28)$$

There is a transformation matrix $\mathbf{T}$ such that $\boldsymbol{A} = \boldsymbol{V_s T}$.

Equation (28) can hence be expressed as:

$$\boldsymbol{J}_2 \boldsymbol{V}_s \boldsymbol{T} = \boldsymbol{J}_1 \boldsymbol{V}_s \boldsymbol{T} \boldsymbol{\Phi} \ldots (29)$$

$$\boldsymbol{J}_2 \boldsymbol{V}_s = \boldsymbol{J}_1 \boldsymbol{V}_s \boldsymbol{T} \boldsymbol{\Phi} \boldsymbol{T}^{-\mathbf{1}} \ldots (30)$$

Define a new matrix $\boldsymbol{\Psi} = \boldsymbol{T\Phi T}^{-\mathbf{1}}$. Substituting $\boldsymbol{\Psi}$ into Equation (30):

$$\boldsymbol{J}_2 \boldsymbol{V}_s = \boldsymbol{J}_1 \boldsymbol{V}_s \boldsymbol{\Psi} \ldots (31)$$

The matrix $\boldsymbol{\Psi}$ is created from the matrix $\boldsymbol{\Phi}$ by a transformation that preserves the eigenvalues. Since the diagonal matrix $\boldsymbol{\Phi}$ has eigenvalues of $e^{-j\frac{2\pi d sin\theta}{\lambda}}$, a DOA estimate can be performed using:

$$\boldsymbol{\Psi} = (\boldsymbol{J}_1 \boldsymbol{V}_s)^{-1} \boldsymbol{J}_2 \boldsymbol{V}_s \ldots (32)$$

$$\phi_i = \arcsin\left(-\frac{\lambda \arg\left(eigvalues(\boldsymbol{\Psi})\right)}{2\pi d}\right) \ldots (33)$$

2.7 Analysis of Simulation Results

MATLAB simulations are performed on the narrowband problem using the MUSIC and ESPRIT Algorithm. The Root Mean Square Error (RMSE) and Mean Square Error (MSE) are the performance metrics used to evaluate the DOA algorithms.

$$MSE = E\left(\left(\hat{\theta} - \theta\right)^2\right) = \frac{1}{n}\sum_{i=1}^{n}\left(\hat{\theta}_i - \theta\right)^2 \dots (34)$$

$$RMSE = \sqrt{E\left(\left(\hat{\theta} - \theta\right)^2\right)} \dots (35)$$

(a) Temporal and Spatial Samples

The results in Figure 4 shows that the accuracy of any subspace based method is dependent on the number of spatial and temporal samples available in the computation of the spatial covariance matrix.

In this simulation model, the DOA of the signal is set at 45 degrees to the broadside of a 2-element ULA, with an inter-element spacing of half the carrier wavelength. The Signal to Noise Ratio (SNR) is set at 0 dB. The estimated DOA is computed from the MUSIC algorithm. The simulation stops when the MSE converges to a unique value. This is repeated with different number of temporal samples. The simulation results show that as the number of temporal samples increases, the MSE decreases.

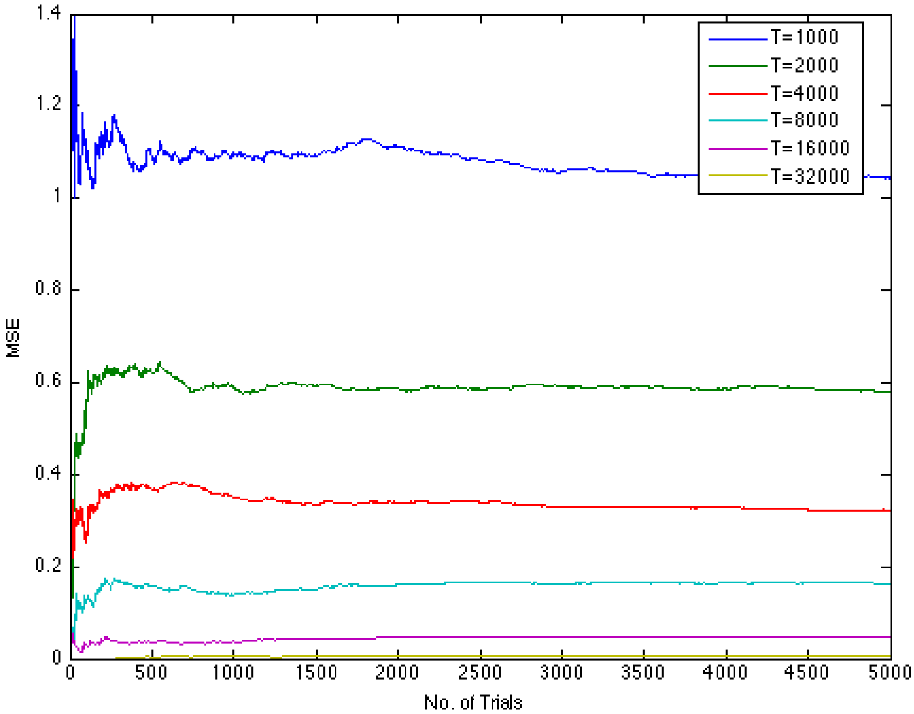

Figure 4: Convergence of MSE for different Temporal Samples T

Table 1: MSE values of different Temporal Samples T

T	MSE
1000	1.0440
2000	0.5796
4000	0.3228
8000	0.1624
16000	0.0474
32000	0.0056
100000	0

If there are a limited number of temporal samples, more spatial samples can be taken to reduce the MSE. The amount of spatial samples T is fixed at 1000 with the same simulation model. The simulation is repeated for different numbers of antenna elements M. Simulation results show that as the number of antennas elements M increases, the MSE decreases.

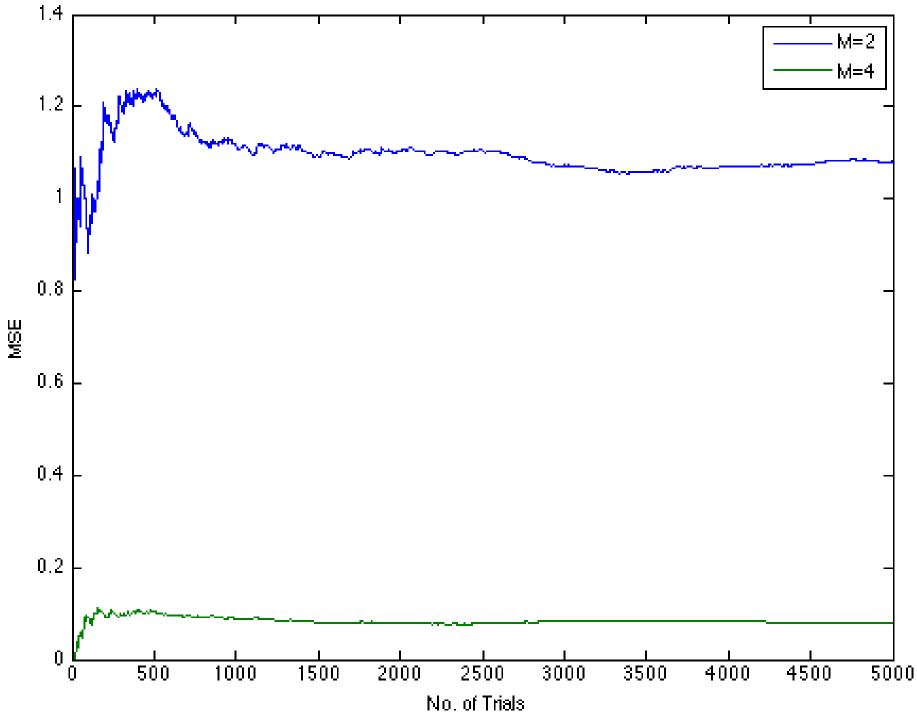

Figure 5: Convergence of MSE for different Spatial Samples M

Table 2: MSE values of different Spatial Samples M

M	MSE
2	1.0440
4	0.0812

(b) MUSIC Algorithm

The MUSIC algorithm is evaluated by simulating a far-field point source with different angles of arrival. The algorithm searches for a DOA at an interval of 1 degree. A quantization error of 0.5 degrees can be expected. In this simulation, the receiver is formed by a 3-element ULA with an inter-element spacing of half the carrier wavelength. The simulation is specified to start at a DOA of -85 degrees and to end at 85 degrees. The number of temporal samples taken to compute the covariance matrix is set at 16,000. It is assumed that the receiver has a SNR of 5 dB. The RMSE associated with each DOA is recorded after it converges at 2000th trial.

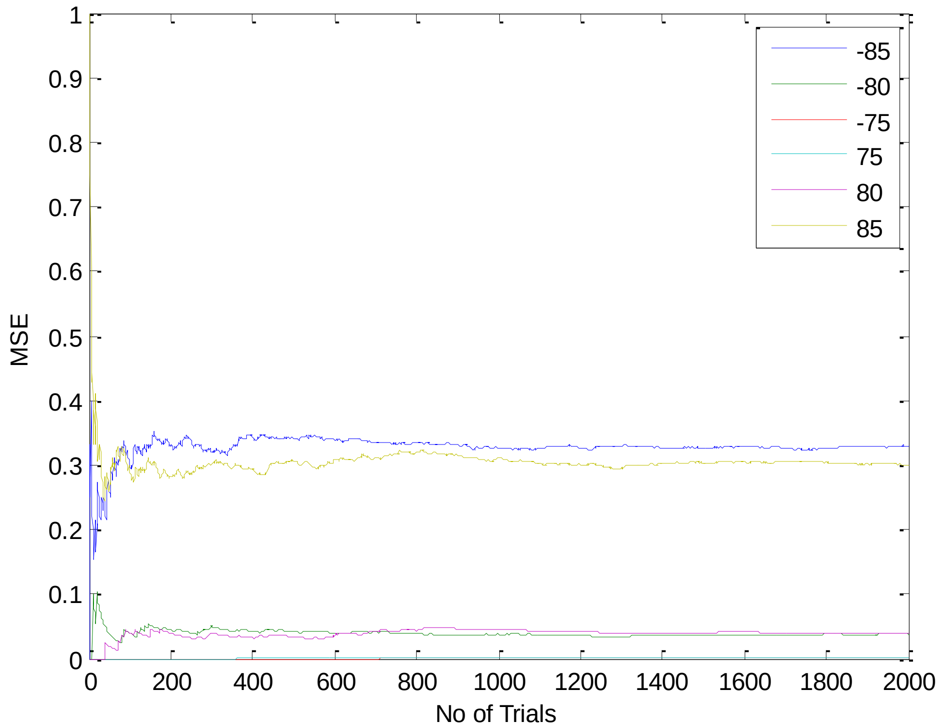

Figure 6: Convergence of MSE in Narrowband MUSIC

Results show that a perfect DOA estimation can be achieved if the signal lies between -65 and 65 degrees. The RMSE increases as the signal approaches the end fire of the ULA. This can be expected because the main beam of the antenna array is at the broadside.

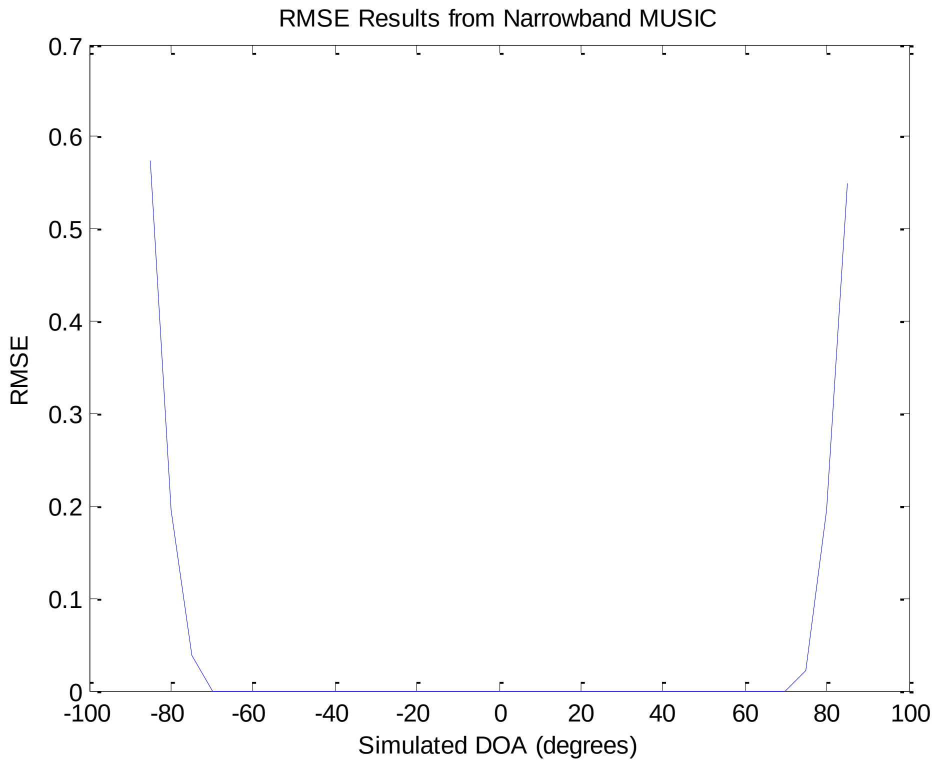

Figure 7: RMSE Results of Narrowband MUSIC

The simulation is also conducted for two specific cases. Figure 9 shows two peaks of different magnitudes, indicating DOAs from two different sources. The more distinct peak at 10 degrees suggests that this DOA is more orthogonal to the noise subspace.

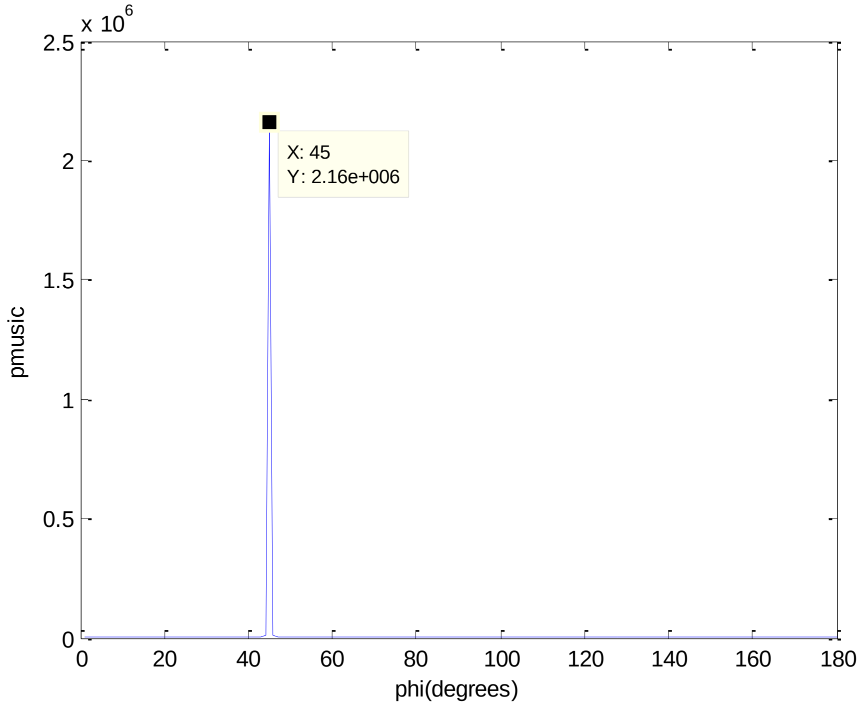

Figure 8: Narrowband MUSIC, M = 2, $\widehat{D} = 1, \theta = 45°$

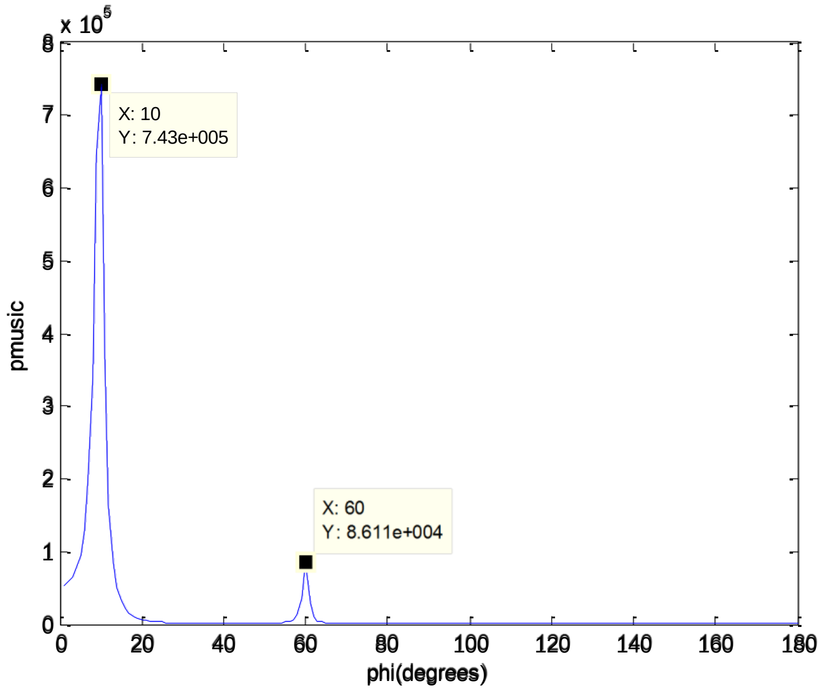

Figure 9: Narrowband MUSIC, M = 3, $\widehat{D} = 2, \theta = 10°, 60°$

(c) ESPRIT Algorithm

The same set of parameters is used in the simulation of the ESPRIT algorithm. The results presented in Figure 10 follow the same trend as the MUSIC algorithm. The DOA computed is most accurate at broadside and least accurate at end fire.

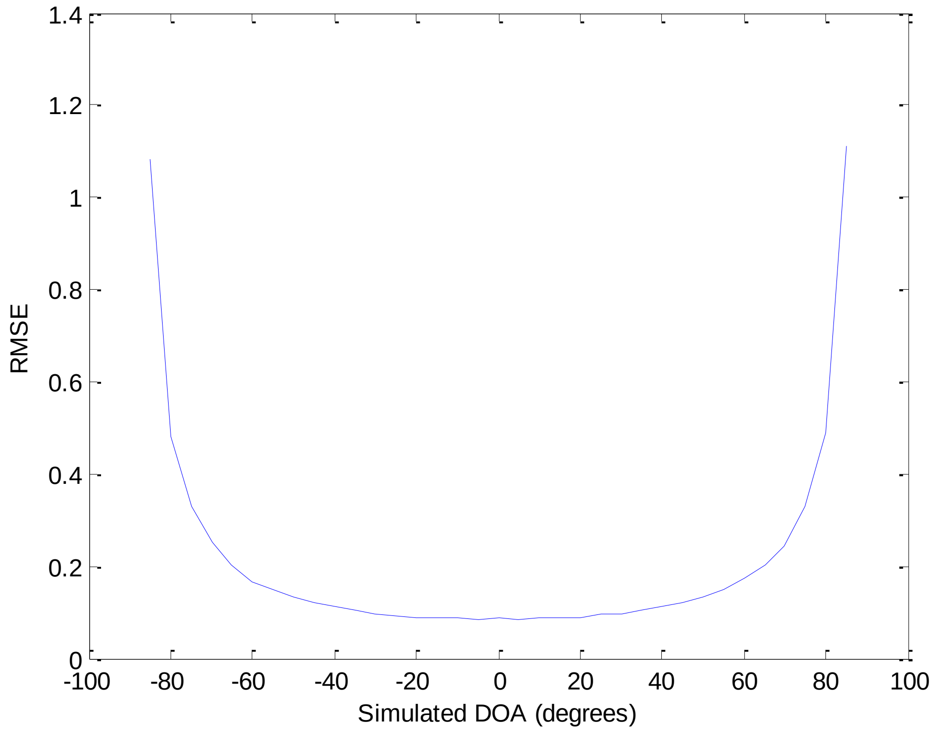

Figure 10: RMSE Results of Narrowband ESPRIT

This model can be extended to multiple sources. A 4 element ULA is simulated to find the DOA of two signals at 35 and 80 degrees. The DOA estimates from the ESPRIT algorithm are 35.2 and 79.8 degrees respectively. An estimation error of 0.2 degrees is observed.

CHAPTER THREE

Direction Finding in Electromagnetic Domain

In this chapter, the wideband problem is first formulated in the frequency domain. The proposed wideband direction finding methods are then presented. The effectiveness of the proposed methods, Maximum Ratio Combining (MRC) and Median Filtering, are evaluated in two practical scenarios: frequency selective fading and narrowband interferences. Finally, an experimental design that validates the narrowband MUSIC algorithm is presented.

3.1 Wideband Signal Model

A wideband signal is filtered at both the transmitter and receiver. In order to emulate this practical design, the random signal generated is passed into a shaping filter. Fast Fourier Transform (FFT) is then applied to obtain the receiver's frequency spectrums at different snapshots of time.

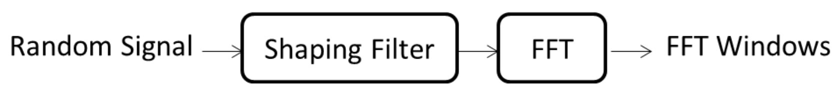

Figure 11: Generating a Wideband Signal (Transmitter Block)

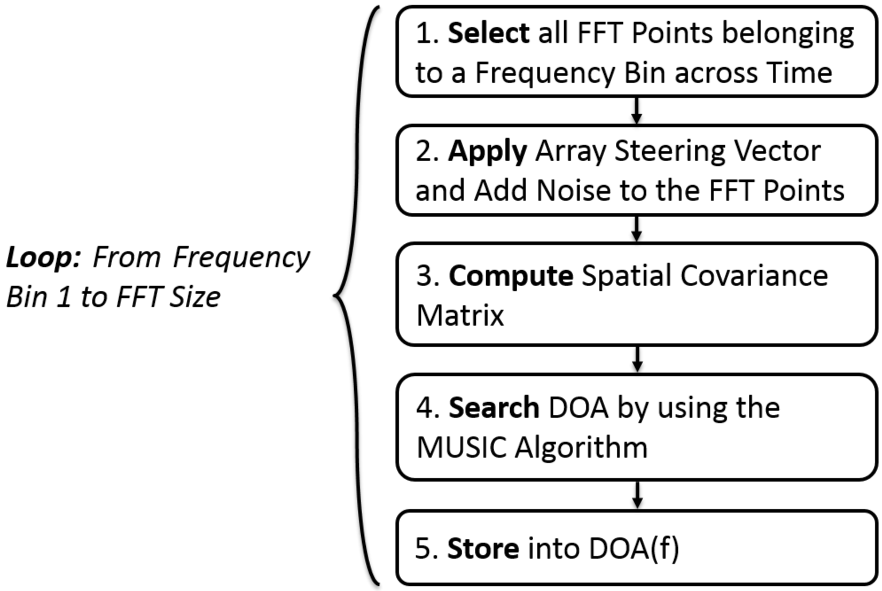

Figure 12: DOA Computation of a Wideband Signal (Receiver Block)

A specific frequency bin, b_i, is selected from the frequency spectrum. b_i contains a range of FFT points obtained at each snapshot of time. Then, the following computations are performed at each point: the array steering vector is multiplied to each point associated with b_i, and noise is added to obtain the received signal vector across time. The spatial covariance matrix is computed and the MUSIC algorithm will search for a DOA corresponding to that frequency bin. This is repeated for all frequency bins such that a vector of DOAs $\theta(f)$ corresponding to the different frequency bins is obtained. This is similar to the narrowband approach except that the steering vector depends on the frequency of the FFT bin and not the carrier frequency.

3.2 Frequency Selective Model

The transmitted wideband signal is filtered through a frequency selective channel. In the simulation, the channel filter is cascaded after applying the shaping filter. The frequency response plot shows that the signal is attenuated differently across all frequency bins. This model is used to evaluate the effectiveness of MRC.

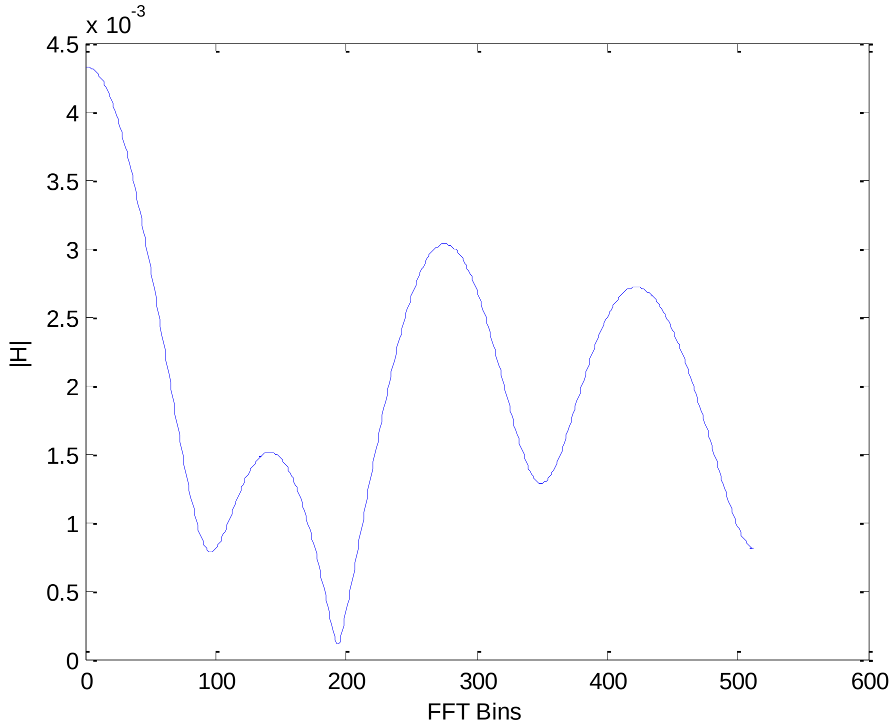

Figure 13: Frequency Response of a Frequency Selective Channel

3.3 Narrowband Interference Model

In an interference free channel, the received spectrum contains the spectral contents from the desired signal $S(f)$ and the noise floor $N(f)$. However, narrowband interferences with a spectrum of $I(f)$ may be present. The receiver will acquire a spectrum that is the sum of $S(f), N\ (f)$ and $I(f)$ instead. At certain FFT bins, these narrowband interferences of a different direction are introduced to the system.

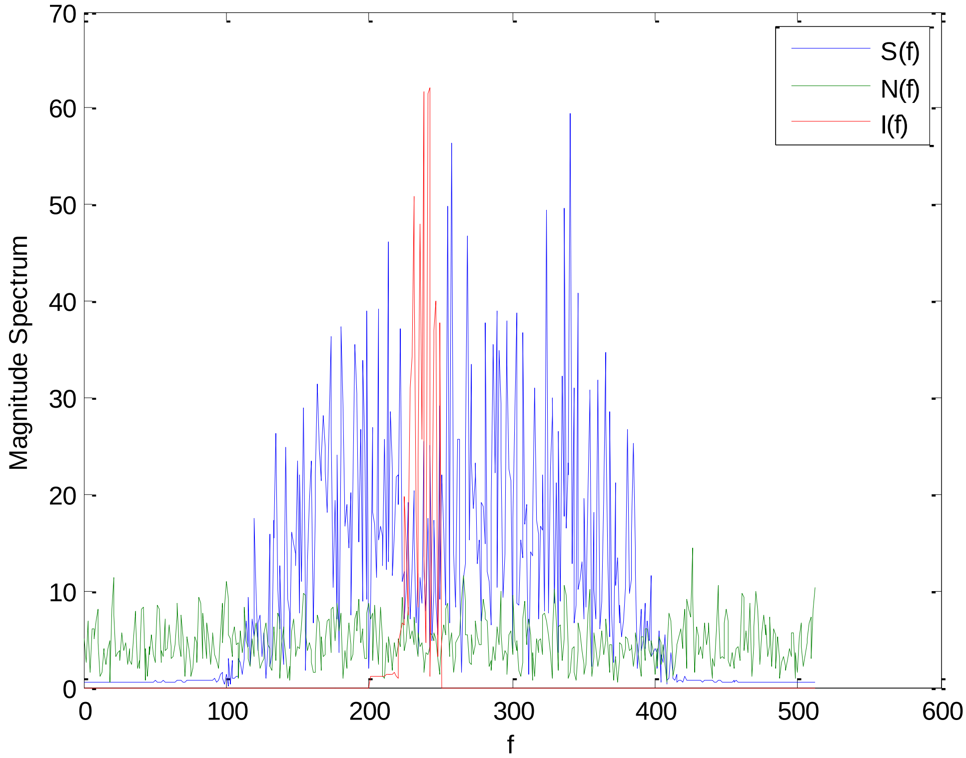

Figure 14: Magnitude Spectrums of Desired Signal, Noise and Interference

3.4 Equal Gain Combining (EGC)

The Incoherent Signal Subspace Method (ISSM) is described as one of the simplest wideband direction finding method. [5] ISSM uses subspace-based methods such as MUSIC to obtain a vector of DOA results within the bandwidth and Equal Gain Combining (EGC) to obtain the final DOA result. This is achieved by averaging the DOA obtained from a FFT size of N.

$$\Theta_{EG} = \frac{1}{N}\sum_{f=1}^{N} \theta(f) \ldots (36)$$

This existing algorithm may not be appropriate in the event of frequency selective fading and narrowband interferences. Maximum Ratio Combining and Median Filtering are proposed to mitigate these effects. These methods seek to improve the DOA estimates obtained from the MUSIC algorithm.

3.5 Maximum Ratio Combining (MRC)

A wideband signal is likely to experience frequency selective fading. This will cause each FFT bin to have a different Signal to Noise Ratio (SNR). Using MRC, frequency bins with a higher SNR value is given more weightage in the final DOA computation. The power $S\,(f)$ can be determined by averaging the diagonals of the covariance matrix.

$$\Theta_{MRC} = \frac{\int S(f)\theta(f)df}{\int S(f)df} \ldots (37)$$

3.6 Median Filtering

If there are narrowband interferences, MRC will allocate significantly more weightage to jammed frequencies. This will result in an inaccurate DOA estimation. Outlier estimates due to narrowband interferences can be reduced with a median filter. If the desired signal DOA is 10 degrees, interference between 151st to 200th FFT bins will result in a wrong DOA estimation at that interval. Using a median filter, these DOA errors can be corrected before EGC is applied.

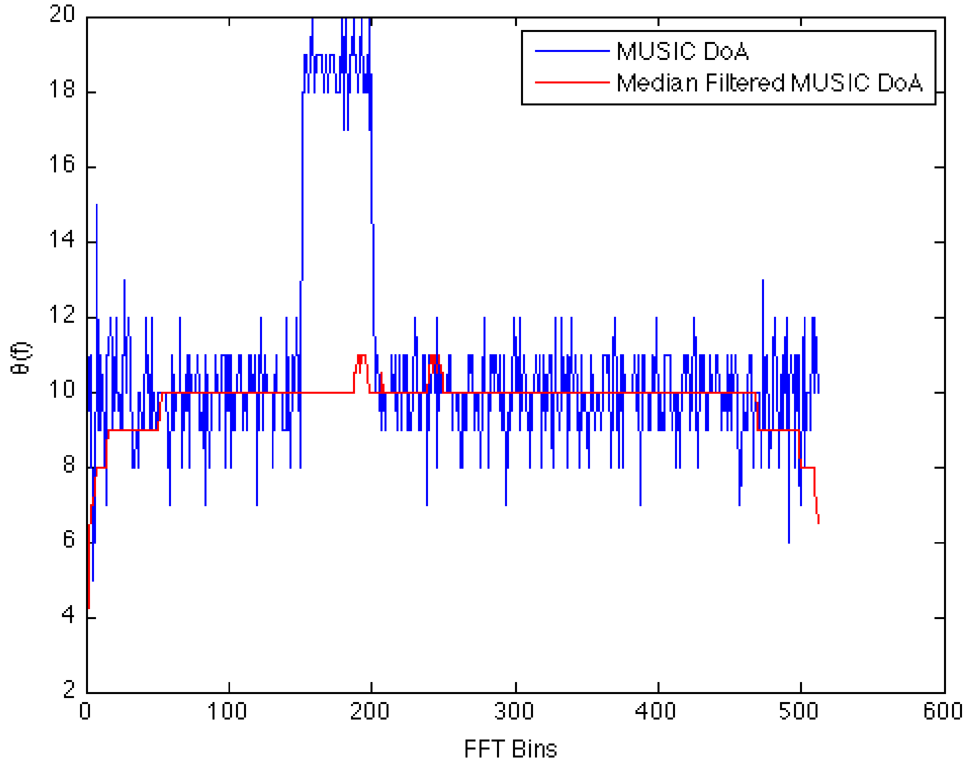

Figure 15: $\theta\ (f)$ Estimate with and without Median Filtering

3.7 Analysis of Simulation Results

In this simulation model, the angle of arrival is 10 degrees. The fractional bandwidth and FFT size are set at 10% and 512 respectively.

(a) Frequency Selective Fading

MRC is compared with EGC in a frequency selective model at different SNR. Simulation results show that MRC is consistently more accurate than EGC. This difference in the MSE results is more distinct at a lower SNR.

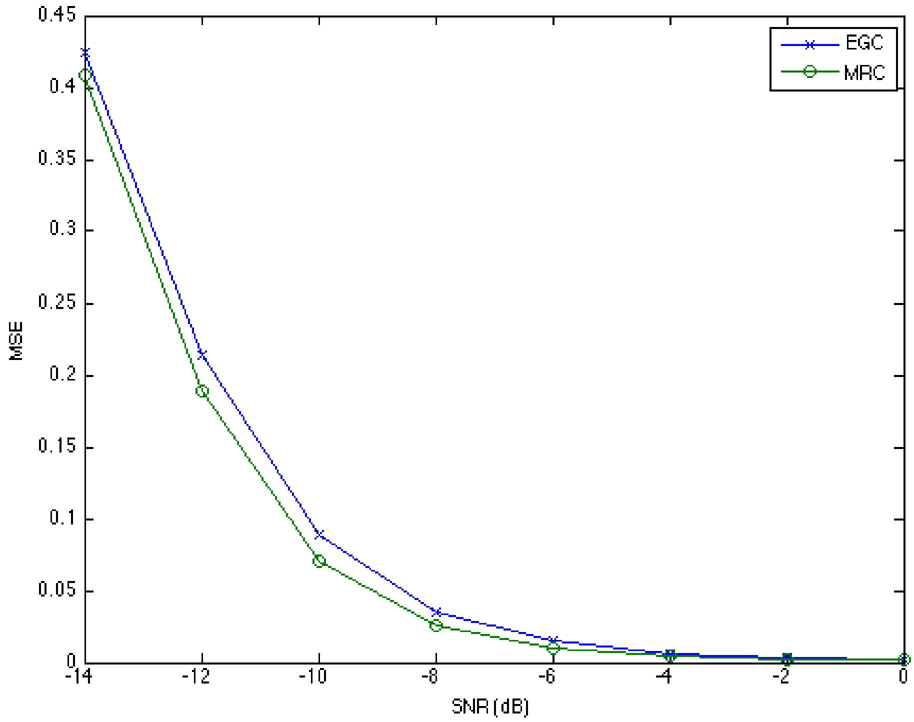

Figure 16: Results from Frequency Selective Model

(b) Narrowband Interferences

Median filtering is compared with MRC and EGC using the narrowband interference model. The MSE is computed across a range of interference bandwidth denoted by the number of FFT points with interference. A SNR of 5 dB is also assumed.

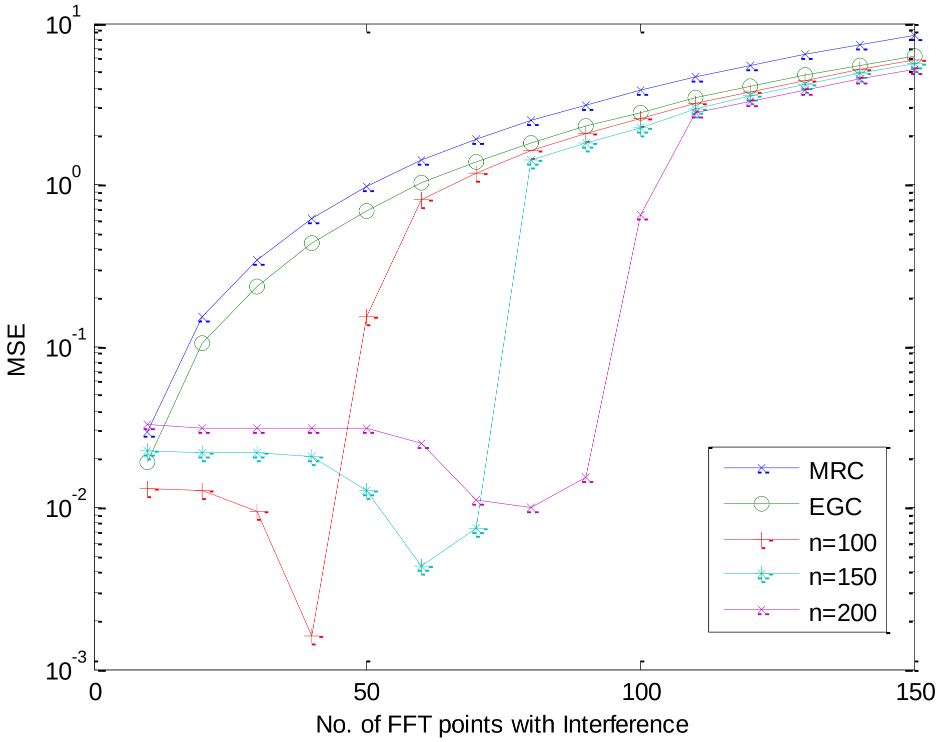

Figure 17: Results from Narrowband Interference Model

Simulation results show that the MRC approach is less accurate in comparison to EGC. This is because more weightage is given to the higher power FFT bins where the interference exists. It can be observed that both MRC and EGC can tolerate a certain amount of narrowband interference. This is because a wideband source offers resistance against intended or unintended jamming. Three median filters with different types of window size *n* are used. It is observed that the MSE is reduced when median filtering is applied. The results suggest that the bandwidth of these narrowband interferences should not exceed half of the median filter's window.

3.8 Experimental Design

An experiment has been designed to validate the narrowband MUSIC algorithm. In this set-up, the signal is emitted from a dipole using a Rhode & Schwarz SMBV100A vector signal generator set at a carrier frequency of 1.575 GHz. A ULA composed of 2 dipole antennas are connected to the Universal Software Radio Peripheral (USRP). The USRP samples the received symbols, and this information is transferred to a Personal Computer (PC) operating MATLAB Simulink.

(a) Floor plan of Antenna Test Chamber

Direction Finding requires a controlled spatial environment during the experimentation process. Figure 18 outlines the top-down view of the proposed hardware set-up. The experiment is conducted in the Antenna Test Chamber of Temasek Laboratories.

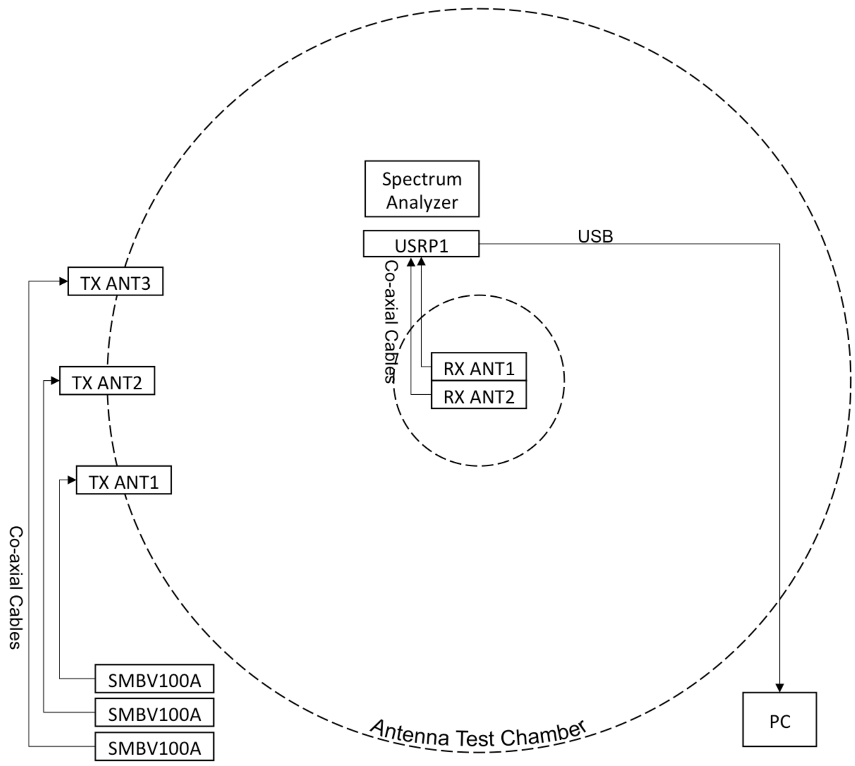

Figure 18: Floor Plan of the Antenna Test Chamber

(b) Phase Calibration

The USRP introduces phase ambiguity upon every initialization. Hence, phase synchronization has to be performed between the 2 input ports. A carrier waveform is transmitted and the phase offset is estimated from the sampled signal S_1 and S_2.

$$\theta_{offset} = arg(\, S_2 * conj(S_1)) \dots (38)$$

A Simulink block code is implemented for phase estimation and compensation. The block code allows for real time observation of the received sampled waveforms. It also allows the user to manually log the data once the phase has been calibrated. It is expected that calibration errors can result in DOA being 2 degrees from the ideal.

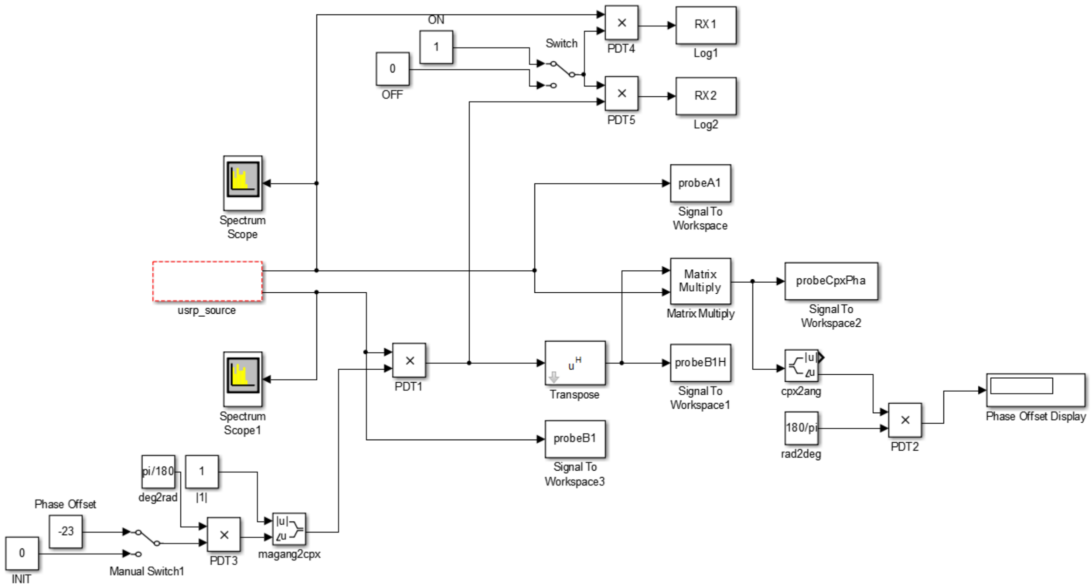

Figure 19: Simulink Block Code

(c) Measured Array Steering Vector

In MATLAB simulations, the path difference is assumed to have negligible impact on the amplitude of the received signal. The MUSIC algorithm is computed using the ideal response of the antenna array. In practical experiments, the measured array steering vector should be used instead. The magnitude and phase response of each antenna element in a 2-element ULA is measured in the Antenna Test Chamber of Temasek Laboratory.

Figure 20: Antenna under Test

From the magnitude response, it is observed that the radiation pattern of each antenna element differs. The radiation pattern of element 1 is symmetrical to that of element 2 about the broadside, or 0 degrees. The inter-element spacing d can also affect the DOA computed. The inter-element spacing should be set to half of its carrier wavelength to reduce mutual coupling.

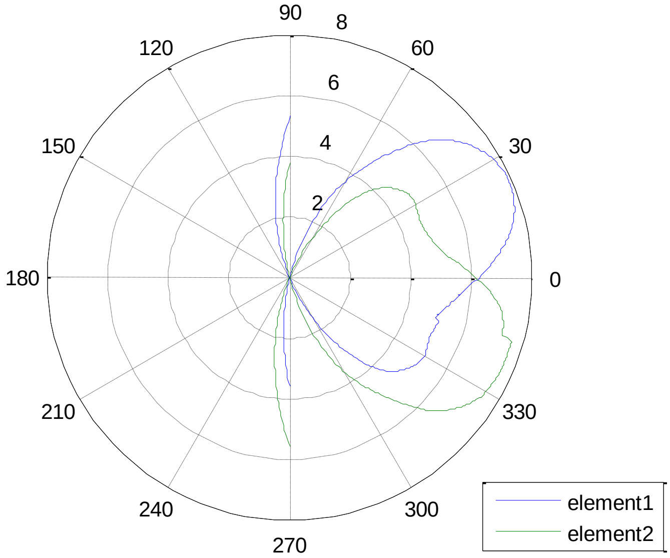

Figure 21: Antenna Radiation Pattern $d = \lambda/2$

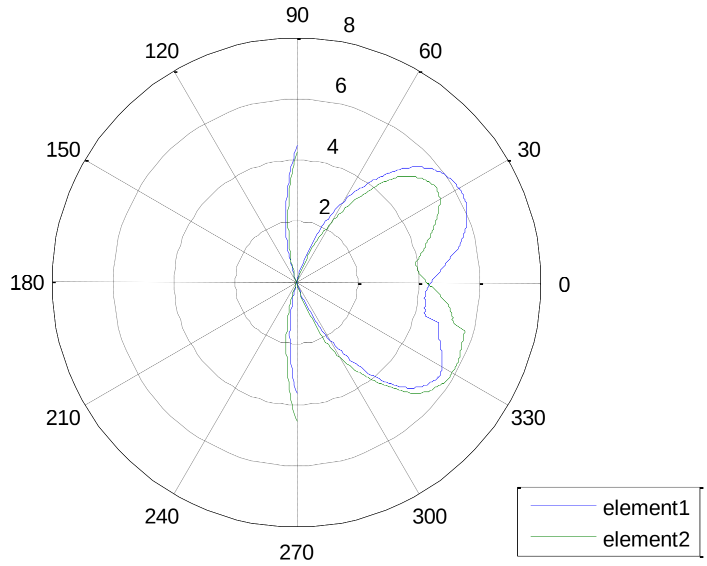

Figure 22: Antenna Radiation Pattern $d = \lambda/4$

The radiation pattern also suggests that an accurate DOA can be achieved if the angle of arrival is within the main lobe. Practical experimentation indicates that the measured array steering vector should be used in the MUSIC algorithm. This is because the measured phase difference does not correspond to the theoretical phase difference computed from the DOA of the source.

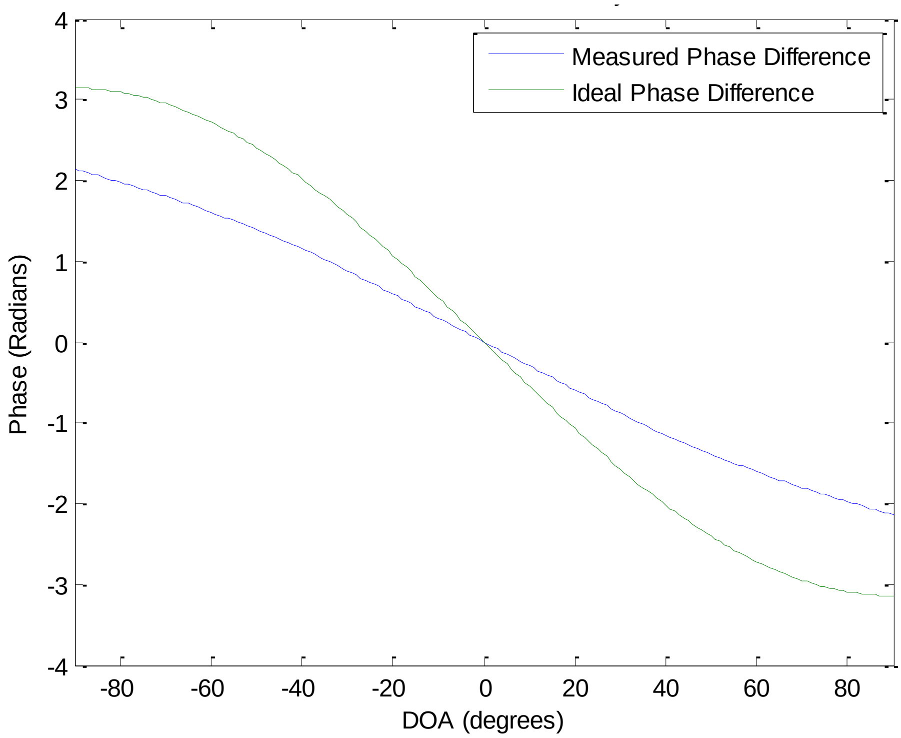

Figure 23: Measured Phase Difference $d = \lambda/2$

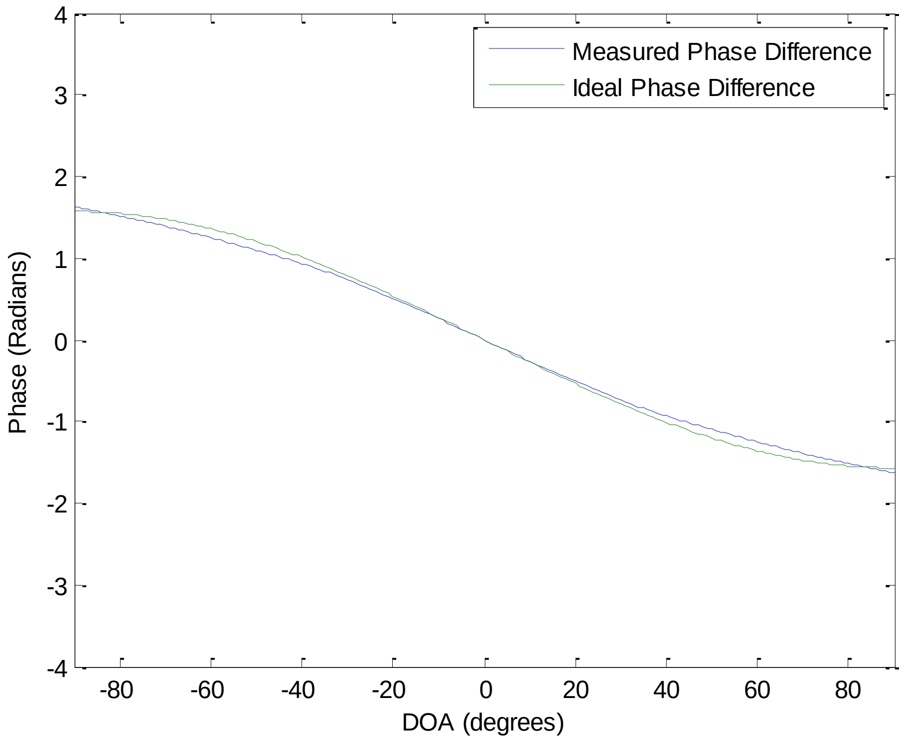

Figure 24: Measured Phase Difference $d = \lambda/4$

The measured array steering vector is stored in a look-up table. Table 3 lists different DOAs and their corresponding measured array steering vectors. The measurement is performed on a ULA with an inter-element spacing of $\lambda/2$, formed by two dipole antennas. For all ϕ, the measured array steering vector should be obtained from Table 3. For example, the array steering vector of $[6.25 + 0.00\mathbf{j}; 6.18 + 0.00\mathbf{j}]$ should be used in the computation of Equation (22) for $\phi = 0\,°$.

Table 3: Measured Array Steering Vector of 2-element ULA, $d = \lambda/2$

DOA	Array Steering Vector
0	[6.25 + 0.00j; 6.18 + 0.00j]
1	[6.35 + 0.00j; 6.02 - 0.66j]
2	[6.47 + 0.00j; 5.79 - 1.29j]
3	[6.58 + 0.00j; 5.50 - 1.88j]
…	…

CHAPTER FOUR

Direction Finding in Acoustic Domain

In this chapter, the hardware design of the AUV's acoustic subsystem is described. The direction finding algorithms are presented with the results obtained from pool tests.

4.1 The Acoustic Waveform

The acoustic pinger emits a pure sinusoidal signal for a short interval of 4 to 10 milliseconds every one second. Although the pinger is a narrowband source, the MUSIC algorithm cannot be directly applied for direction finding. This is because the source does not emit a continuous waveform, and the ping undergoes multipath propagation. Array signal processing techniques are developed such that the MUSIC algorithm can be applied in the acoustic channel.

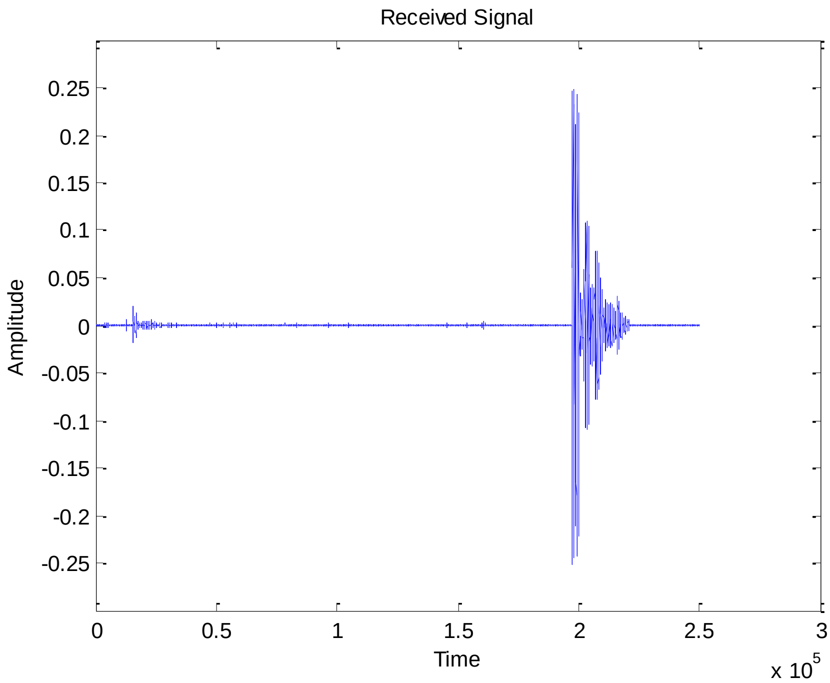

Figure 25: Recorded waveform of an Acoustic Ping

4.2 Hardware Design

The type of hardware available determines the design of the acoustic sub-system and the type of algorithm that can be implemented. This algorithm design is possible because of the sponsorship by National Instruments and the equipment loan from Reson.

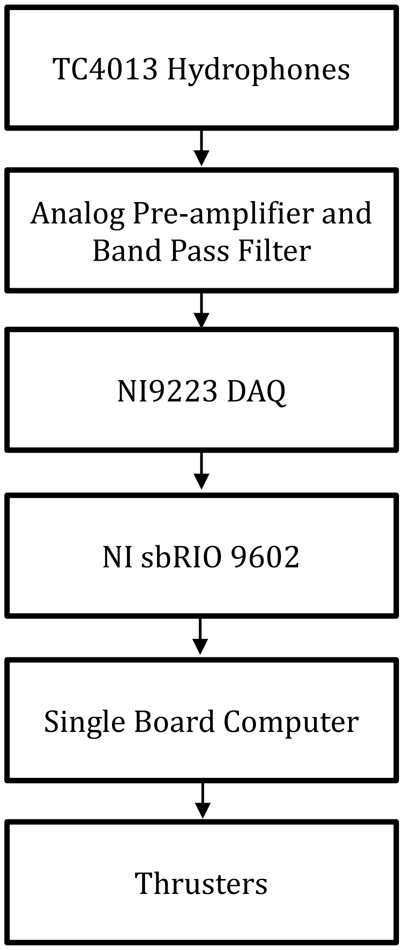

Figure 26: Acoustic System Block Diagram

(a) Hydrophone Array

In order to implement beamforming techniques, the inter-element spacing should not exceed half of the carrier wavelength to avoid spatial aliasing. This means that the hydrophone must be small and compact. The Teledyne Reson's TC4013 hydrophones have a small diameter of 9.5mm. This makes it possible to design a hydrophone array with an inter-element spacing of 1.5cm.

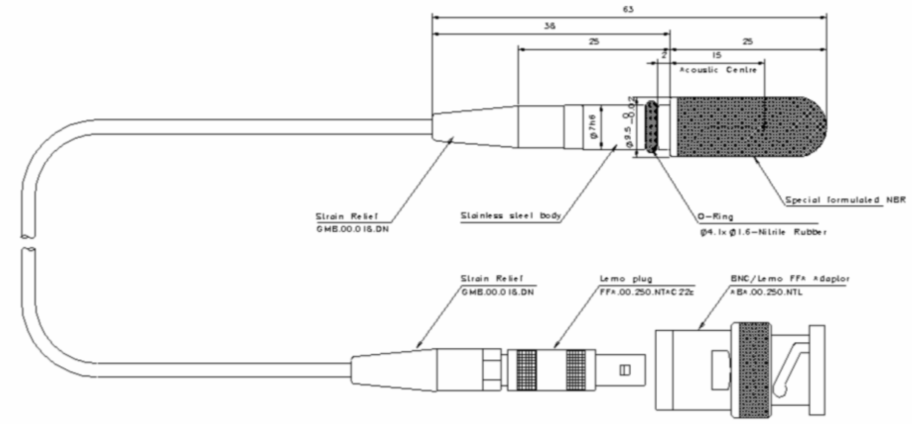

Figure 27: Dimensions of TC4013 Hydrophone

The horizontal directivity pattern of the hydrophone is omni-directional at 100 kHz. A slight deviation of 2 dB can be expected. The omni-directional hydrophone allows the ping to be detected at any azimuth angle between 0 and 360 degrees.

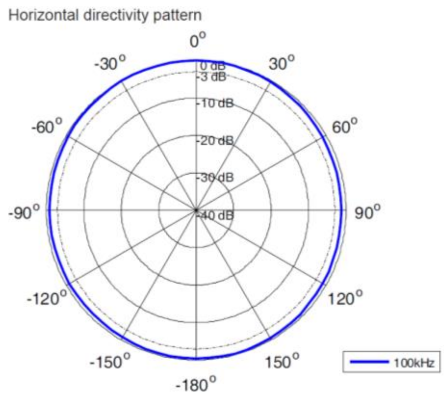

Figure 28: Horizontal Directivity Pattern of TC 4013

The hydrophone array is formed by four hydrophones positioned in a square-formation. This square array allows for DOA computation (Azimuth angle and Elevation angle) in 3-dimensional plane. This design also resolves the front-back ambiguity problem of a ULA. A hydrophone mount is designed on SolidWorks and fabricated precisely using laser-cutting technology.

Figure 29: Design of Hydrophone Mount

(b) Analog Pre-amplifier and Band Pass Filter

There is no built-in pre-amplifier in the TC4013 hydrophone. A low current pre-amplifier and band pass filter board is designed. This is fabricated on a double-layer printed circuit board using surface mount devices. The amplified analog signal is passed through a band pass filter which attenuates the unwanted frequency components before sampling is done in the digital domain. The board has been characterized by a bode plot.

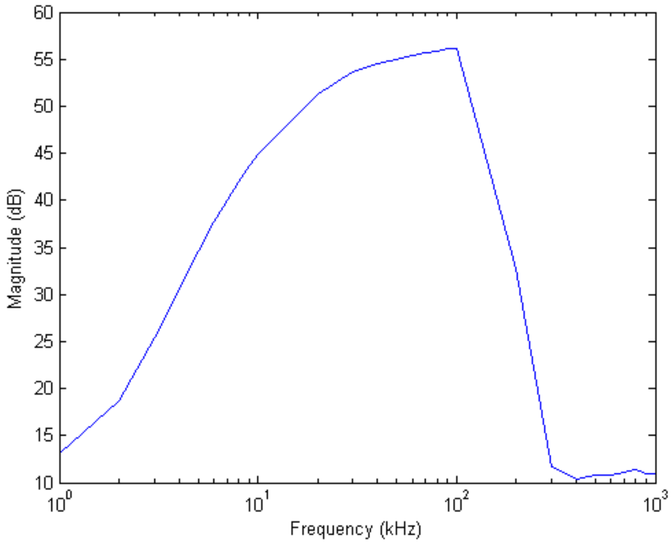

Figure 30: Frequency Response plot of the implemented Band pass Filter

(c) Analog to Digital Converter

The four channel outputs from the pre-amplifier and band pass filter boards are sampled using National Instruments NI9223 Analog Input Module (DAQ). This module can sample at a maximum rate of 1MS/s/channel simultaneously. In order to recover the signal emitted by the pinger, the sampling rate of this DAQ is set at 250k samples per second.

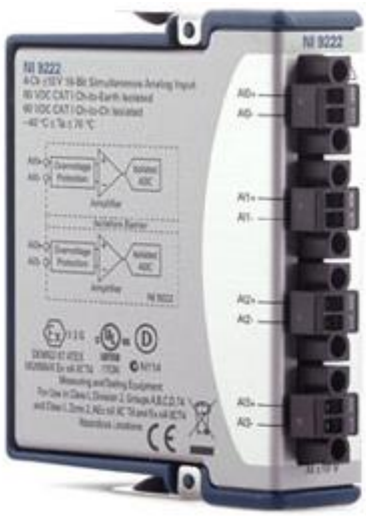

Figure 31: NI9223 DAQ Module

(d) Field Programmable Gate Array (FPGA)

Array signal processing is performed on sampled inputs using National Instruments sbRIO NI9206. Elliptic band pass filtering, dynamic thresholding and Fast Fourier Transform (FFT) are programmed on the FPGA using Labview 2012.

Figure 32: NI sbRIO-9602/9602XT

(e) Single-Board Computer

The FPGA communicates with the AUV's Single-Board Computer (SBC) using the TCP-IP protocol. The SBC is an Intel Ivy Bridge Core i7-3610QE processor mounted on the EMB-QM77 Motherboard. The sophisticated beamforming algorithms are implemented this SBC.

4.3 Algorithm Design

There are four unique components in the algorithm design. These include digital filtering, peak and dynamic threshold detection, signal extraction and Fast Fourier Transform, and the high resolution MUSIC algorithm.

(a) 10^{th} Order Band pass Filtering

The sampled signal is passed through an elliptic 10^{th} order band pass filter with a center frequency set at the desired frequency of the ping. This digital filter has a narrow 3 dB bandwidth of 5 kHz. The filter is designed to ensure sufficient attenuation to frequency components that are 7.5 kHz from its center frequency. This is necessary because the algorithm must be able to correctly detect and differentiate between two acoustic pings at 37.5 kHz and 45 kHz.

(b) Peak and Dynamic Threshold Detection

As the pinger does not emit a carrier waveform continuously, the receiver must identify the start of each ping before information on its phase can be extracted. Peak and dynamic threshold detection is applied to estimate the time of arrival of each ping. Dynamic thresholding is preferred over simple thresholding because the received power is inversely proportional to the distance between the pinger and the hydrophone array. The dynamic threshold is computed by scaling the maximum amplitude of the received signal by a constant factor.

This approach provides a coarse estimation in the time of arrival. The use of high-resolution beamforming techniques does not require an extremely accurate time of arrival estimate because the DOA information of the acoustic source is carried in the phase differences of the ping. This resolves the existing problem in the TDOA algorithm.

The TDOA algorithm requires an accurate time of arrival estimate for direction finding. This is difficult to achieve because the peak and dynamic threshold detection does not optimally estimate an accurate time of arrival.

(c) Signal Extraction and Fast Fourier Transform

Upon identifying the start of a ping, only the initial segment is extracted for post processing. Due to multipath reverberations, only this initial segment originates from the line of sight signal. When the multipath effect sets in at the later stages, the ping becomes distorted and a stable phase cannot be obtained. Hence, it is necessary to extract the initial segment of the ping so that an accurate DOA can be computed. The amount of samples extracted is defined by a size that corresponds to the FFT size. From extensive experimentation, an appropriate FFT size is 128 when the sampling frequency is 250 kHz.

From this extracted signal, FFT-operations are performed to check if the identified signal falls within the desired frequency range of the pinger. If this condition is satisfied, the complex numbers (FFT points) associated with the peaks of the power spectrum are extracted. These FFT points are used in the high-resolution beamforming algorithm.

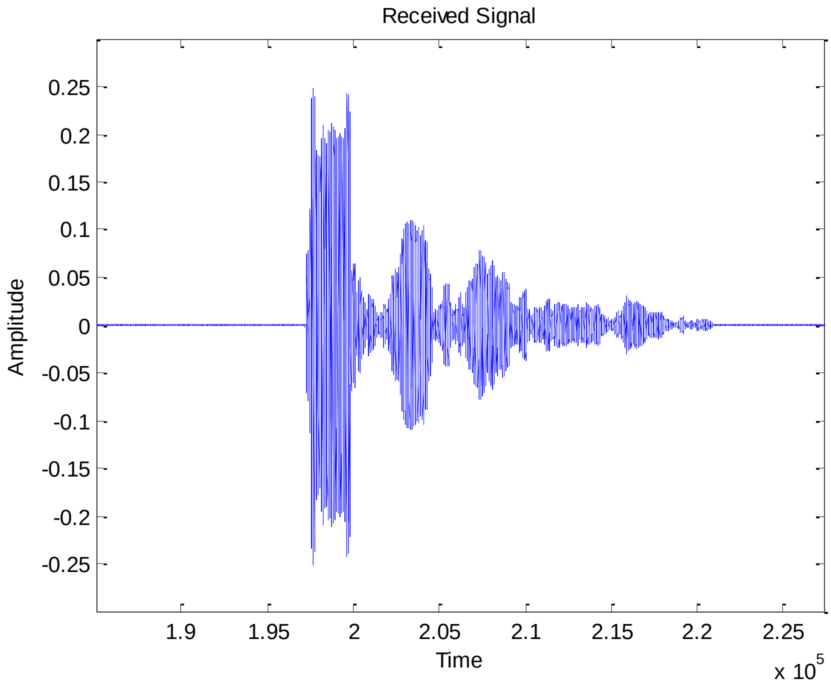

Figure 33: Multipath Reverberation on the received Acoustic Ping

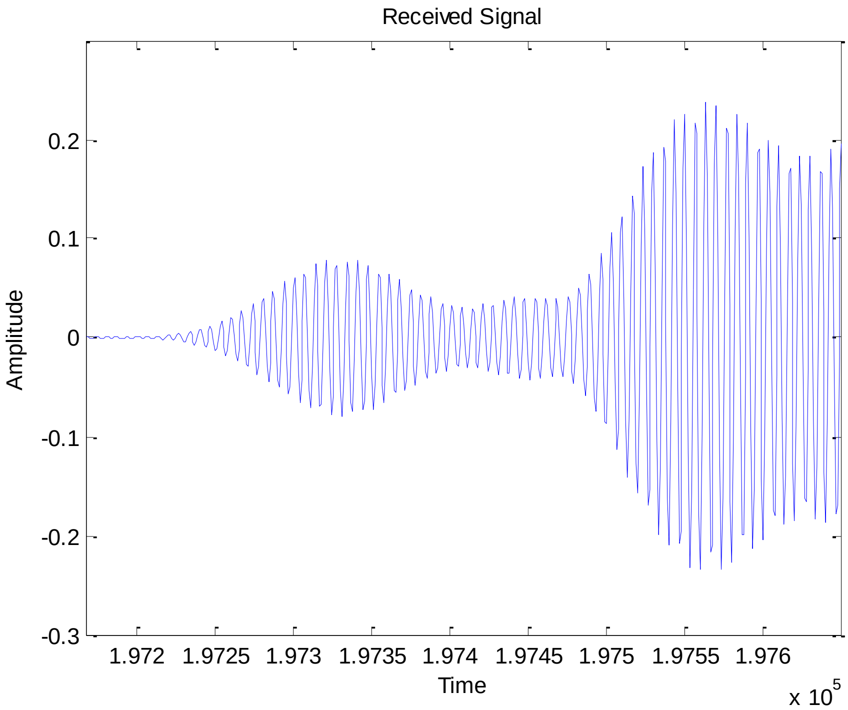

Figure 34: Initial Segment of an Acoustic ping

(d) High Resolution Beamforming: MUSIC Algorithm

MUSIC is chosen as the high-resolution beamforming algorithm for acoustic source localization. In this application, the spatial covariance matrix is computed from the FFT points extracted over a period of 3 pings. The MUSIC algorithm searches for a set of azimuth θ and elevation angle ϕ where the array steering vector is the most orthogonal to the noise eigenvectors $\boldsymbol{V_n}$.

$$\alpha(\phi,\theta) = \begin{bmatrix} \exp\left(\frac{j2\pi r}{\lambda} sin\phi\, cos(\theta - 45)\right) \\ \exp\left(\frac{j2\pi r}{\lambda} sin\phi\, cos(\theta + 45)\right) \\ \exp\left(\frac{j2\pi r}{\lambda} sin\phi\, cos(\theta + 135)\right) \\ \exp\left(\frac{j2\pi r}{\lambda} sin\phi\, cos(\theta + 225)\right) \end{bmatrix} \dots (39)$$

$$\widehat{\boldsymbol{P}}_{\boldsymbol{music}}(\phi,\theta) = \frac{\boldsymbol{\alpha^H}(\phi,\theta)\boldsymbol{\alpha}(\phi,\theta)}{\boldsymbol{\alpha^H}(\phi,\theta)\boldsymbol{V_n}\boldsymbol{V_n^H}\boldsymbol{\alpha}(\phi,\theta)} \dots (40)$$

4.4 Analysis of Pool Test Results

The acoustic localization algorithm has been tested extensively in the pool and the relevant results are recorded. The experiments were conducted at a depth of 1.8m. The pingers are positioned 4 meters away from the hydrophone array. The 200 series transponder (BCN-0200-8000/4) from Applied Acoustic Engineering is set up as a pinger.

The pinger is positioned at different azimuth angles between -80 and 80 degrees to the broadside. The hydrophone array and the pinger are placed at a depth of 1m. The elevation angle is ignored in the following experimental analysis because it is difficult to model this parameter given the limited depth of the pool.

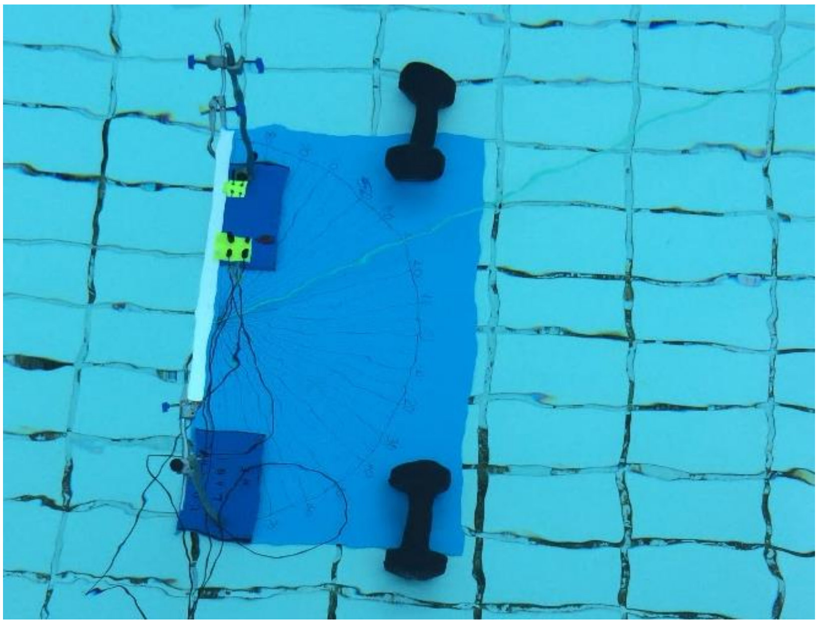

Figure 35: Pool Test Set-up

The MUSIC algorithm is first compared with the phase difference method. Instead of a square array, the phase difference method is computed from a 2-element ULA. The phase difference Θ_{mn} between hydrophone *m* and *n* is:

$$\Theta_{mn} = \arg(Z_m Z_n{}^*) \ldots (41)$$

This phase difference is due to the path difference (l_{mn}) between the 2 parallel wavefronts. Hence, the DOA θ can be computed.

$$l_{mn} = dsin\theta_{mn} \ldots (42)$$

$$\Theta_{mn} = \frac{2\pi dsin\theta_{mn}}{\lambda_c} \ldots (43)$$

$$\theta_{mn} = asin\left(\frac{\frac{v_{water}}{f_c} \times \Theta_{mn}}{2\pi d}\right) \ldots (44)$$

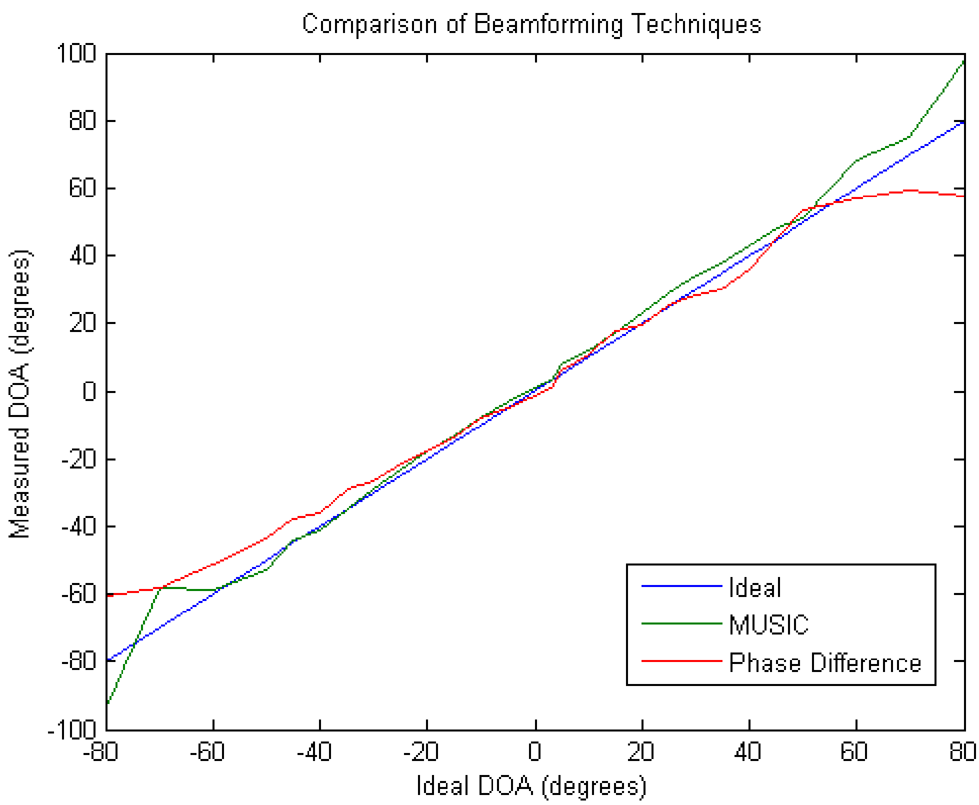

Figure 36: Comparison between MUSIC and Phase Difference

Table 4: RMSE Results from Pool Tests

	MUSIC	Phase Difference
RMSE	5.791	7.388

Results show that the sophisticated MUSIC algorithm yields a lower Root Mean Square Error (RMSE) compared to the simpler phase difference method. The RMSE measured from the MUSIC algorithm is 5.8 degrees. In contrast, the phase difference method yields a poorer RMSE result of 7.4 degrees.

Since the MUSIC algorithm computes the DOA based on more spatial samples from the square array, it is not surprising that a better DOA result is achieved. This improvement in DOA result is also contributed by the symmetrical property of a square array. The symmetrical property allows for accurate DOAs to be computed consistently over a range of angles.

The asymmetric ULA is a reason why a good estimate cannot be consistently achieved with the phase difference method. It is observed that the DOA estimate has the most deviation from the ideal DOA when the pinger is at the end-fire of the ULA. A good estimate can be obtained only if the signal is at the broadside of the ULA.

Since it is difficult to extend the simpler phase difference method to a square array, the high resolution MUSIC algorithm is preferred. It has been shown that the MUSIC algorithm is able to consistently deliver an accurate DOA estimate.

Thus, it is worthwhile to adopt this algorithm since the AUV has the computational power and capacity to do so.

The accuracy of the MUSIC algorithm is constrained by the time of arrival estimate. While it does not require a correct time of arrival estimate from the peak and dynamic threshold detection, an inaccurate DOA estimate will result if the detection estimates a time of arrival corresponding to the reflected pings. This is because an inconsistent phase is extracted from the power spectrum.

Apart from the MUSIC algorithm, other beamforming techniques can be considered. The Fourier method is commonly known as the classical beamformer or the delay-and-sum method. The Fourier method searches for a DOA such that the output power is the maximum.

$$\boldsymbol{P_{cbf}}(\phi, \theta) = \alpha^{H}(\phi, \theta)\mathbf{R}\alpha(\phi, \theta) \dots (45)$$

The results of the Fourier method are very similar to the MUSIC algorithm. The RMSE of both the MUSIC and Fourier methods is approximately 5.8 degrees. It is observed that a distinct peak is obtained from the MUSIC algorithm. In contrast, the Fourier method has a less distinct peak.

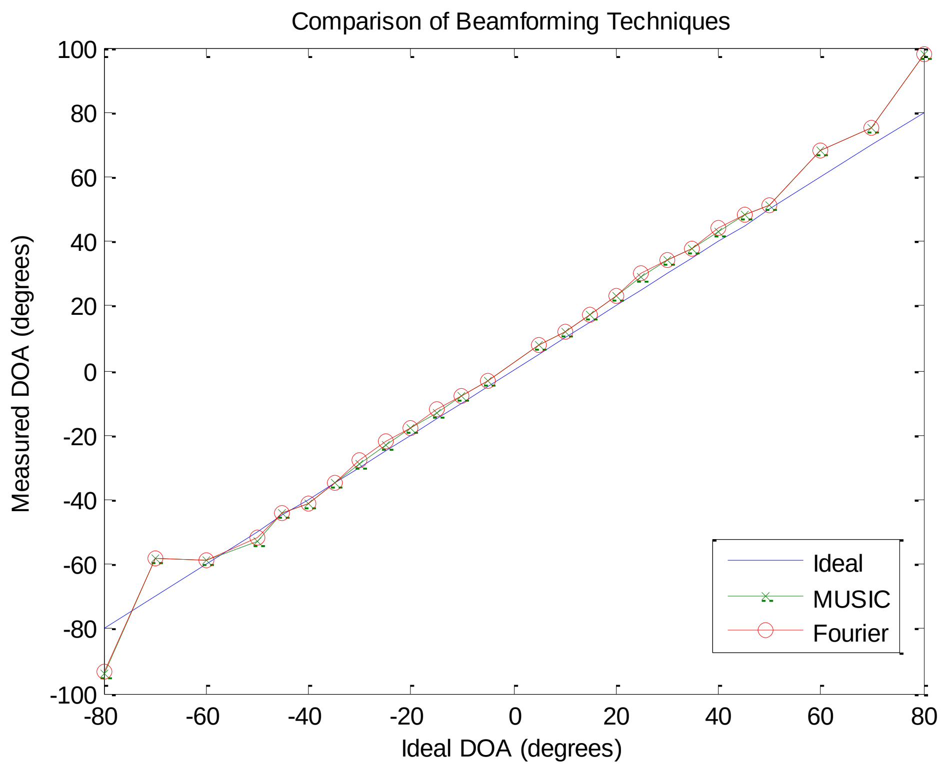

Figure 37: Comparison between MUSIC and Fourier

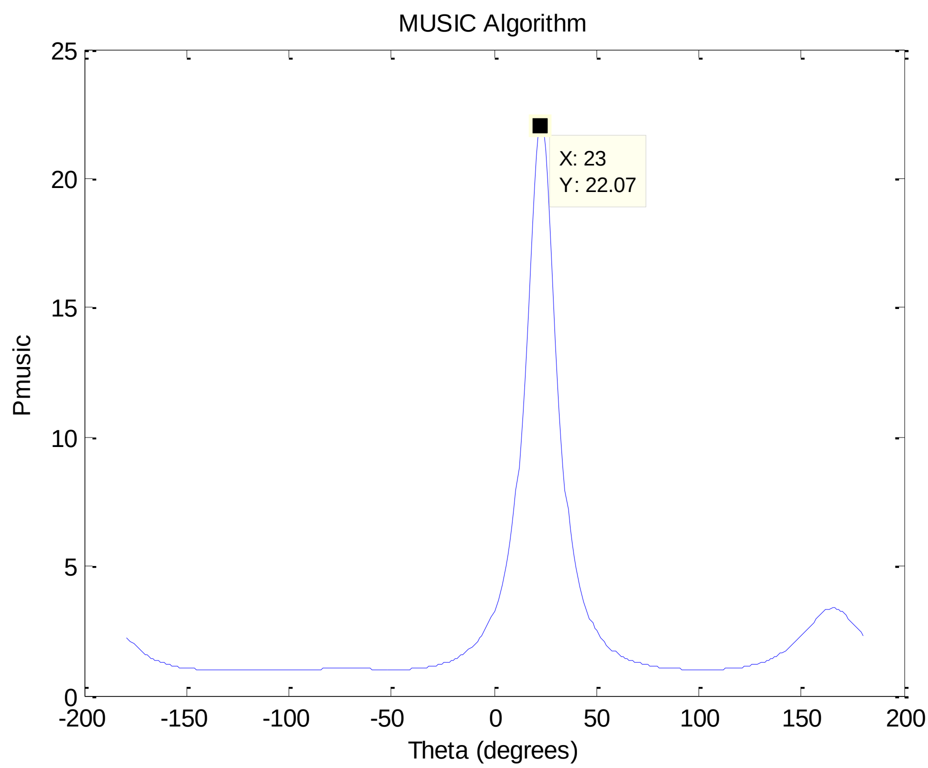

Figure 38: Plot of $\hat{P}_{music}(\phi)$ computed when ideal DOA is 20 degrees

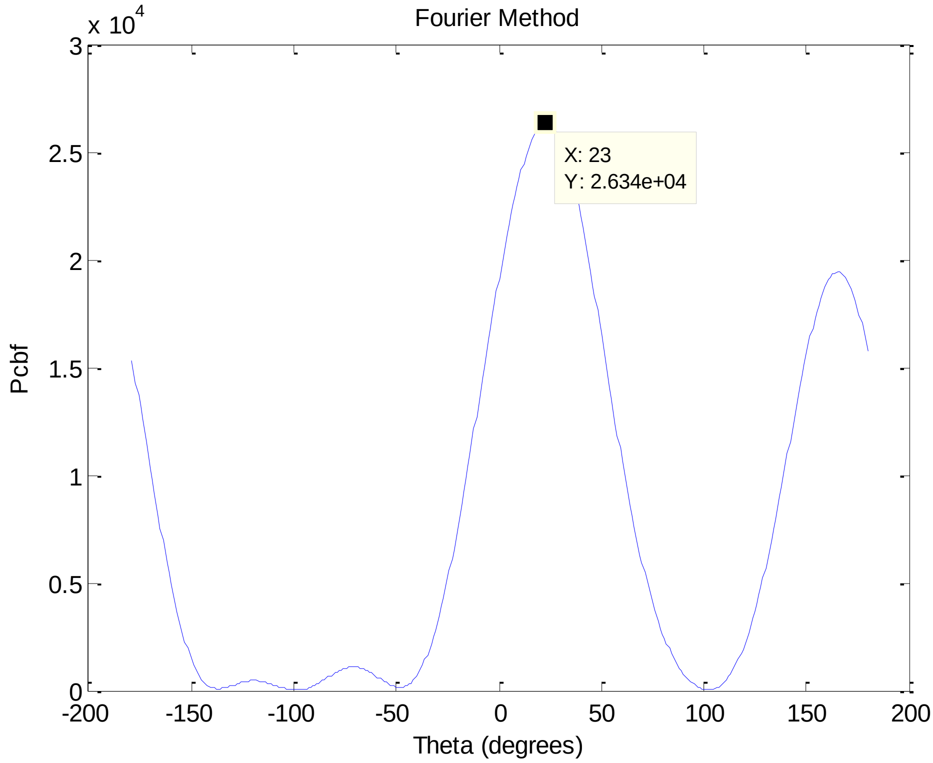

Figure 39: Plot of $P_{cbf}(\phi)$ computed when ideal DOA is 20 degrees

4.5 System Integration

The functional acoustic sub-system has been integrated on the Bumblebee Autonomous Underwater Vehicle (BBAUV). The needs and requirements of the mechanical, electrical and software sub-systems have to be taken into account during the integration process.

(a) Mechanical

A dedicated acoustic housing has been designed and fabricated by the mechanical engineering students in the team. The electrical hardware routing has to accommodate the mechanical design constraints.

(b) Software

The direction finding algorithm is integrated into the Mission Planner which simultaneously runs multiple nodes. The Mission Planner only initiates the Acoustic Node upon completion of the other tasks. In the unlikely event where the AUV is unable to complete the current tasks, the Mission Planner will transit to the Acoustic Node as a fall back plan. Recognizing that node transitions can occur at any spatial coordinates, it is worthwhile to maneuver the AUV to an optimum listening post before direction finding is done. This reduces the spatial uncertainty when the AUV is in autonomous mode.

At the listening post, the AUV will hover and acquire the signal emitted by the first pinger. The AUV computes its relative direction to the pinger with the MUSIC algorithm and turns to face it. It then moves forward by a pre-defined step size, and hover and listen for the next ping. This is repeated until the elevation angle suggests that the pinger is directly above the AUV.

Upon localizing the first pinger, the AUV will search for the direction of the second pinger. Since the second pinger is of a fixed distance away from the first pinger, its precise location can be known by just its direction once the first pinger has been localized. The AUV will then move to the midpoint of these pingers and surface, completing the task.

CHAPTER FIVE

Conclusion

In this thesis, sophisticated direction finding techniques have been proposed in practical scenarios from the acoustic and electromagnetic domain. Each algorithm is designed specifically based on the waveform of the transmitter as well as the form of channel impairment present. The direction finding problem has been studied through theoretical simulations and laboratory experimentations. A functional acoustic sub-system has also been designed on an AUV.

The main contributions made to the field of wideband direction finding include Maximum Ratio Combining for a frequency selective channel and Median Filtering for narrowband interferences. These contributions can be applied to spread spectrum signals in the field of wireless communication. One of the motivations for using spreading codes is to provide a form of resistance to intended interference and jamming by the enemy. Direction finding and beamforming can then provide an additional layer of protection to the signal in the spatial domain.

Array signal processing and the high-resolution beamforming algorithms have been applied in the acoustic domain. Much effort is devoted to the hardware and algorithm design. Pool test results suggest that a good DOA estimate can be achieved from the MUSIC algorithm using a square array. This design has been integrated onboard an AUV to complete the acoustic localization task in SAUVC.

There remain practical problems unaddressed in this thesis. These include the implementation of a real-time direction finding system and validating the proposed wideband algorithms through laboratory experiments and field tests. Furthermore, this thesis only studied two of the many configurations of antenna arrays for direction finding -- the Uniform Linear Array and square array. As each configuration exhibits a unique radiation pattern, the accuracy of the DOA computed from the high-resolution beamforming algorithms can vary with configuration. These effects are not examined in this thesis and should be considered for future works.

REFERENCES

[1] M. V. Hamid Krim, "Two Decades of Array Signal Processing Research," *IEEE Signal Processing Magazine*, pp. 67-94, 1996.

[2] L. D. Stone, "Search for the Underwater Wreckage of Air France Flight 447," in *Proceedings of 14th International Conference on Information Fusion*, Chicago, 2011.

[3] IEEE OES Singapore Chapter, "The Singapore AUV Challenge," 2014. [Online]. Available: http://ewh.ieee.org/r10/singapore/oes/sauvc/index.html. [Accessed 1 December 2013].

[4] AUVSIfoundation, "RoboSub - Foundation," Association for Unmanned Vehicle Systems International, [Online]. Available: http://www.auvsifoundation.org/foundation/competitions/robosub/. [Accessed 20 March 2014].

[5] L. M. K. J. H. M. Yeo-Sun Yoon, "TOPS: New DOA Estimator for Wideband Signals," *IEEE Transactions on Signal Processing*, vol. 54, no. 6, pp. 1977-1989, 2006.

[6] R. P. Elio D. Di Claudio, "WAVES: Weighted Average of Signal Subspaces for Robust Wideband Direction Finding," *IEEE Transactions on Signal Processing*, vol. 49, no. 10, pp. 2179-2191, 2001.

[7] BBAUV, "Passive Sonar System - BUMBLEBEE AUV," [Online]. Available: http://www.bbauv.com/vehicles/2013-2/electrical/acoustics/. [Accessed 1 December 2013].

[8] M. Bartlett, "Smoothing Periodograms from Time Series with Continuous Spectra," *Nature,* vol. 161, pp. 686-687, 1 May 1948.

[9] J. Capon, "High Resolution Frequency-Wavenumber Spectrum Analysis," *Proceedings of the IEEE,* vol. 57, no. 8, pp. 1408-1418, August 1969.

[10] L. K. Georges Bienvenu, "Adaptivity to Background Noise Spatial Coherence for High Resolution Passive Methods," *IEEE,* pp. 307-310, 1980.

[11] M. S. Haihua Chen, "On Non-Uniqueness of Stochastic ML Estimation of DOA and its best solution," *Proceedings of 2007 International Symposium on Intelligent Signal Processing and Commnication Systems,* pp. 372-375, 2007.

[12] T. K. Richard Roy, "ESPRIT - Estimation of Signal Parameters Via Rotational Invariance Techniques," *IEEE Transactions on Acoustics Speech and Signal Processing,* vol. 37, no. 7, pp. 984-995, 1989.

[13] T.-J. S. T. K. Mati Wax, "Spatio-Temporal Spectral Analysis by Eigenstructure Methods," *IEEE Transactions on Acoustics, Speech and Signal Processing,* Vols. ASSP-32, no. 4, pp. 817-827, 1984.

[14] M. G. B. Allen, Adaptive Array Systems, West Sussex, England: Wiley, 2005.

[15] T. S. D. (Shendkar), "Application of MUSIC, ESPRIT and ROOT MUSIC in DOA Estimation," Faculty of Electrical Engineering and Computing, University of Zagreb, Croatia.

[16] T. K. Richard Roy, "ESPRIT - Estimation of Signal Parameters Via Rotational Invariance Techniques," *IEEE Transactions on Acoustic, Speech and Signal Processing,* vol. 37, no. 7, pp. 984-995, 1989.

APPENDIX A

Spatial Covariance Matrix

A Simplified Signal Model:

$$\begin{pmatrix} r_1 \\ r_2 \\ r_3 \end{pmatrix} = \begin{pmatrix} e^{-j\omega\tau} \\ e^{-2j\omega\tau} \\ e^{-3j\omega\tau} \end{pmatrix} S_1 + \begin{pmatrix} N_1 \\ N_2 \\ N_3 \end{pmatrix}$$

Expected Value of Sum is Sum of Expected Value:

$$\begin{pmatrix} E(r_1) \\ E(r_2) \\ E(r_3) \end{pmatrix} = \begin{pmatrix} E\left(e^{-j\omega\tau}\right) \\ E\left(e^{-2j\omega\tau}\right) \\ E\left(e^{-3j\omega\tau}\right) \end{pmatrix} S_1 + \begin{pmatrix} E(N_1) \\ E(N_2) \\ E(N_3) \end{pmatrix}$$

Since there is a Deterministic Signal:

$$\begin{pmatrix} E(r_1) \\ E(r_2) \\ E(r_3) \end{pmatrix} = \begin{pmatrix} S_1 e^{-j\omega\tau} \\ S_1 e^{-2j\omega\tau} \\ S_1 e^{-3j\omega\tau} \end{pmatrix} + \begin{pmatrix} E(N_1) \\ E(N_2) \\ E(N_3) \end{pmatrix} = \begin{pmatrix} S_1 e^{-j\omega\tau} + E(N_1) \\ S_1 e^{-2j\omega\tau} + E(N_2) \\ S_1 e^{-3j\omega\tau} + E(N_3) \end{pmatrix}$$

Covariance Matrix of the Received Signal Vector is defined as such:

$$R_x = \begin{pmatrix} E(r_1) \\ E(r_2) \\ E(r_3) \end{pmatrix} \begin{pmatrix} E(r_1) \\ E(r_2) \\ E(r_3) \end{pmatrix}^H$$

$$= \begin{pmatrix} S_1 e^{-j\omega\tau} + E(N_1) \\ S_1 e^{-2j\omega\tau} + E(N_2) \\ S_1 e^{-3j\omega\tau} + E(N_3) \end{pmatrix} \begin{pmatrix} S_1 e^{j\omega\tau} + E(N_1)^* & S_1 e^{2j\omega\tau} + E(N_2)^* & S_1 e^{3j\omega\tau} + E(N_3)^* \end{pmatrix}$$

$$= \begin{pmatrix} {S_1}^2 + {\sigma_1}^2 & {S_1}^2 e^{j\omega\tau} & {S_1}^2 e^{2j\omega\tau} \\ {S_1}^2 e^{-j\omega\tau} & {S_1}^2 + {\sigma_2}^2 & {S_1}^2 e^{j\omega\tau} \\ {S_1}^2 e^{-2j\omega\tau} & {S_1}^2 e^{-j\omega\tau} & {S_1}^2 + {\sigma_3}^2 \end{pmatrix}$$

Proof:

$For\ m\ \neq k, where\ m\ and\ k\ are\ integers:$

$$E(N_m)^* = E(N_m) = E(N_k)^* = E(N_k) = 0\ (AWGN)$$

$$E(N_m)E(N_k)^* = 0\ (independent)$$

$$\left(S_1 e^{-jm\omega\tau} + E(N_m)\right)\left(S_1 e^{jm\omega\tau} + E(N_m)^*\right)$$

$$= {S_1}^2 + S_1 e^{jm\omega\tau} E(N_m) + S_1 e^{-jm\omega\tau} E(N_m)^* + E(N_m)^* E(N_m)$$

$$= {S_1}^2 + E(N_m)^* E(N_m)$$

$$= {S_1}^2 + {\sigma_m}^2$$

$$\left(S_1 e^{-jm\omega\tau} + E(N_m)\right)\left(S_1 e^{jn\omega\tau} + E(N_n)^*\right) =$$

$$= {S_1}^2 e^{j(n-m)\omega\tau} + S_1 e^{jn\omega\tau} E(N_m) + S_1 e^{-jm\omega\tau} E(N_n)^* + E(N_m)E(N_n)^*$$

$$= {S_1}^2 e^{j(n-m)\omega\tau}$$

Simplifying the Covariance Matrix:

$$R_x = \begin{pmatrix} {S_1}^2 & {S_1}^2 e^{j\omega\tau} & {S_1}^2 e^{2j\omega\tau} \\ {S_1}^2 e^{-j\omega\tau} & {S_1}^2 & {S_1}^2 e^{j\omega\tau} \\ {S_1}^2 e^{-2j\omega\tau} & {S_1}^2 e^{-j\omega\tau} & {S_1}^2 \end{pmatrix} + \begin{pmatrix} {\sigma_1}^2 & 0 & 0 \\ 0 & {\sigma_2}^2 & 0 \\ 0 & 0 & {\sigma_3}^2 \end{pmatrix}$$

If ${\sigma_1}^2 = {\sigma_2}^2 = {\sigma_3}^2 = \sigma^2$

$$R_x = {S_1}^2 \begin{pmatrix} 1 & e^{j\omega\tau} & e^{2j\omega\tau} \\ e^{-j\omega\tau} & 1 & e^{j\omega\tau} \\ e^{-2j\omega\tau} & e^{-j\omega\tau} & 1 \end{pmatrix} + \begin{pmatrix} \sigma^2 & 0 & 0 \\ 0 & \sigma^2 & 0 \\ 0 & 0 & \sigma^2 \end{pmatrix}$$

$$R_x = {S_1}^2 \begin{pmatrix} 1 & e^{j\omega\tau} & e^{2j\omega\tau} \\ e^{-j\omega\tau} & 1 & e^{j\omega\tau} \\ e^{-2j\omega\tau} & e^{-j\omega\tau} & 1 \end{pmatrix} + \sigma^2 \begin{pmatrix} 1 & 0 & 0 \\ 0 & 1 & 0 \\ 0 & 0 & 1 \end{pmatrix}$$

Recall that the Array Steering Vector is $A = \begin{pmatrix} e^{-j\omega\tau} \\ e^{-2j\omega\tau} \\ e^{-3j\omega\tau} \end{pmatrix}$

$$R_A = \begin{pmatrix} e^{-j\omega\tau} \\ e^{-2j\omega\tau} \\ e^{-3j\omega\tau} \end{pmatrix} \begin{pmatrix} e^{-j\omega\tau} \\ e^{-2j\omega\tau} \\ e^{-3j\omega\tau} \end{pmatrix}^H = \begin{pmatrix} e^{-j\omega\tau} \\ e^{-2j\omega\tau} \\ e^{-3j\omega\tau} \end{pmatrix} \begin{pmatrix} e^{j\omega\tau} & e^{2j\omega\tau} & e^{3j\omega\tau} \end{pmatrix}$$

$$R_A = \begin{pmatrix} 1 & e^{j\omega\tau} & e^{2j\omega\tau} \\ e^{-j\omega\tau} & 1 & e^{j\omega\tau} \\ e^{-2j\omega\tau} & e^{-j\omega\tau} & 1 \end{pmatrix}$$

Key Result: $\mathbf{R_x} = \mathbf{R_A} + \sigma^2\mathbf{I}$ assuming that ${S_1}^2 = 1$